AGU PUBLICATIONS

JGR

Journal of Geophysical Research: Earth Surface

RESEARCH ARTICLE

10.1002/2014JF003318

Key Points:
- Footwall relief reflects fault segmentation for the studied faults <60 km long
- Knickpoints are generated by fault linkage and their heights scale with footwall relief
- Fault throw rates calculated from knickpoint heights and footwall relief

Correspondence to:
A. C. Whittaker,
a.whittaker@imperial.ac.uk

Citation:
Whittaker, A. C., and A. S. Walker (2015), Geomorphic constraints on fault throw rates and linkage times: Examples from the Northern Gulf of Evia, Greece, *J. Geophys. Res. Earth Surf.*, *120*, 137–158, doi:10.1002/2014JF003318.

Received 21 AUG 2014
Accepted 8 DEC 2014
Accepted article online 12 DEC 2014
Published online 30 JAN 2015

Geomorphic constraints on fault throw rates and linkage times: Examples from the Northern Gulf of Evia, Greece

Alexander C. Whittaker[1] **and A. Sofia Walker**[1]

[1]Department of Earth Science and Engineering, Royal School of Mines, Imperial College, London, UK

Abstract We evaluate how the growth and interaction of active normal faults in the Sperchios Basin and Northern Gulf of Evia, Greece, are recorded by the landscape. We demonstrate that patterns in footwall relief along the faults reflect fault segmentation, and we show that in this study area, fault throw is 2 to 3 times the maximum footwall relief. Rivers crossing the faults typically have two knickpoints, which are unrelated to lithology. However, their heights, measured from the active fault trace, vary systematically. The height of the upper set of knickpoints scales linearly with the footwall relief of the faults and is typically >85% of the maximum relief. The height of the lower set of knickpoints also scales with footwall relief, but the heights are consistently lower. The existence of two sets of knickpoints suggests that the rivers have been perturbed by two changes in tectonic rates during faulting. We interpret the upper knickpoints to represent the initiation and growth of fault-generated topography, while the lower set of knickpoints reflects a throw rate increase due to fault linkage. Estimates of throw rate enhancement factor derived from fault interaction theory suggest that the faults increased their rate by a factor of ≥3 when they linked. This constraint, combined with the distribution of knickpoint heights, allows us to estimate the throw rate and linkage time for the faults. The Sperchios Fault has a maximum throw rate of 1.5–2.0 mm/yr, while the Coastal Fault has a maximum throw rate of 0.8–1.2 mm/yr.

1. Introduction

It has been widely established that active normal faults have a distinctive topographic expression [e.g., *Anders et al.*, 1993; *Goldsworthy and Jackson*, 2000; *Densmore et al.*, 2003, 2004; *Roberts and Michetti*, 2004; *Walker et al.*, 2010; *Tucker et al.*, 2011; *Papanikolaou et al.*, 2013, and references therein], particularly in terms of their footwall relief [*Densmore et al.*, 2004; *Whittaker et al.*, 2008], control on surrounding drainage networks [e.g., *Cowie et al.*, 2006; *Attal et al.*, 2008], and routing of sediment from catchments to neighboring depocenters [*Eliet and Gawthorpe*, 1995; *Cowie et al.*, 2006; *Whittaker et al.*, 2010; *Forzoni et al.*, 2014]. The clear relationship between active normal faulting and topography raises the prospect of being able to solve the tectonic "inverse problem" [*Wobus et al.*, 2006a; *Roberts and White*, 2010; *Kirby and Whipple*, 2012; *Whittaker*, 2012], in which the slip rates of normal faults are constrained from specific geomorphic observables such as footwall relief, triangular facet, and fault scarp geometry [*Densmore et al.*, 2004, 2007; *Petit et al.*, 2009; *Tucker et al.*, 2011]; channel steepness of footwall streams [*Wobus et al.*, 2006a; *Kirby and Whipple*, 2012; *Whittaker*, 2012]; or the presence and elevation of knickpoints upstream of mapped faults [*Commins et al.*, 2005; *Whittaker et al.*, 2008; *Boulton and Whittaker*, 2009; *Miller et al.*, 2012]. This would allow us to make robust comparisons between fault displacement rates derived from geologic and structural constraints, typically averaged over 10^6–10^7 years [e.g., *Cowie and Roberts*, 2001; *Mirabella et al.*, 2004], with short-term rates derived from geodetic measurements [*Billiris et al.*, 1991, 1997; *Clarke et al.*, 1998], paleoseismic trenching work, and Holocene offsets of fault scarps, terraces, or fans [e.g., *Roberts and Michetti*, 2004; *Pantosti et al.*, 2004; *Walker et al.*, 2010]. As the locus and slip rates of active faults are also directly linked to the presence, size, and frequency of earthquakes [e.g., *Roberts et al.*, 2004], such an approach would enable us to reconcile competing estimates of seismic hazard [*Boulton and Whittaker*, 2009; *Papanikolaou et al.*, 2013] and would particularly be useful in study areas where geologic or geodetic constraints are sparse [*Kirby et al.*, 2003; *Whittaker*, 2012; *Miller et al.*, 2012; *Kirby and Whipple*, 2012].

The analysis of river long profiles in fluvial landscapes has been the primary route for tackling this problem, driven by the burgeoning availability of high-quality digital elevation model (DEM) data in the last 15 years

[*Whipple and Tucker*, 2002; *Tucker and Whipple*, 2002; *Kirby et al*., 2003; *Wobus et al*., 2006a; *Whittaker et al*., 2008; *Kirby and Whipple*, 2012, and references therein]. Rivers are demonstrably sensitive to tectonically controlled base level change through adjustment of their planform geometry and channel steepness [*Finnegan et al*., 2005; *Wobus et al*., 2006c; *Whittaker et al*., 2007a]. Consequently, a multitude of studies have addressed, from theoretical, field, and modeling perspectives, how rivers record active faulting in either topographic steady state [e.g., *Kirby and Whipple*, 2001, 2003, 2006a; *Cyr et al*., 2010] or during a transient response to tectonics, where the rate of fluvial incision does not match fault uplift rates [*Whipple and Tucker*, 2002; *Crosby and Whipple*, 2006; *Whittaker et al*., 2008; *Roberts and White*, 2010; *Miller et al*., 2012; *Whittaker and Boulton*, 2012].

Most of these studies rely on some form of the stream power erosion law [e.g., *Howard and Kerby*, 1983; *Whipple and Tucker*, 2002; *Wobus et al*., 2006a]. In steady state landscapes, where the rate of rock uplift, U, equals the rate of fluvial downcutting, this can be written as

$$U = KA^m S^n, \tag{1}$$

where m and n are the positive exponents that describe the dependency of stream incision rate on drainage area, A, and channel slope, S, and K is a parameter describing erosional efficiency. The latter implicitly includes variables such as rock strength and sediment supply effects [e.g., *Attal et al*., 2008]. Consequently, it is commonplace to write

$$S = \left(\frac{U}{K}\right)^{\frac{1}{n}} A^{\frac{-m}{n}}, \tag{2}$$

where the coefficient $\left(\frac{U}{K}\right)^{\frac{1}{n}} = k_s$, the steepness index of the channel, which depends on uplift rate (and K). As the steepness index and concavity (m/n) covary, normalized steepness k_{sn} is calculated using a reference concavity [*Wobus et al*., 2006a]. Normalized steepness indices have shown a solid correlation with independent measures of uplift rate, erosion rate, or base level fall in a range of areas including the Himalaya [e.g., *Kirby et al*., 2003; *Harkins et al*., 2007; *Ouimet et al*., 2009], the Italian Apennines [*Whittaker et al*., 2008; *Cyr et al*., 2010], and Papua New Guinea [*Miller et al*., 2012]. However, converting k_{sn} values to fault slip rates is not simple because the relationship between k_{sn} and U depends on n and may be linear [e.g., *Kirby et al*., 2003; *Wobus et al*., 2006a] or sublinear [e.g., *Ouimet et al*., 2009; *DiBiase et al*., 2010]. Moreover, channels in topographic steady state can have identical k_{sn} values for significantly different uplift rates [*Whittaker*, 2012], because channel steepness is sensitive to other variables such as lithology, sediment flux, and climate embedded in K [*DiBiase and Whipple*, 2011].

"Bedrock" rivers undergoing a transient erosional response to a change in tectonic rates also embed tectonic information. Theoretical, observational, and modeling studies have shown that when such channels are perturbed by a base level change, such as increased movement on an active fault, a steep transient knickzone develops in the river long profile as it steepens to keep pace with the new boundary conditions [*Tucker and Whipple*, 2002; *Wobus et al*., 2006a; *Whittaker et al*., 2008; *Miller et al*., 2012] (Figure 1a) The knickpoint separates the catchment's downstream section that is incised and adjusted to the new fault throw rate from the upper section that is yet to respond and retains the characteristics of the preexisting state [*Kirby and Whipple*, 2012]. Migration of the knickpoint upstream creates a wave of incision that transmits the signal of boundary condition change to the whole catchment [*Tucker and Whipple*, 2002; *Harkins et al*., 2007; *Whittaker*, 2012] (Figure 1a).

Theoretical considerations [e.g., *Wobus et al*., 2006b] and landscape evolution models [e.g., *Attal et al*., 2008] suggest that the vertical rate of knickpoint propagation through a landscape should be independent of catchment size and discharge but should relate to the relative uplift rate perturbation experienced by the channel as it crosses a fault [*Crosby and Whipple*, 2006; *Whittaker et al*., 2008]. The heights of knickpoints created by an increase in fault throw rate therefore increase over time. This is shown schematically in Figure 1b for a river channel evolving from time t_0 to t_5 after a threefold increase in fault throw rate. The height of knickpoints upstream of an active fault, should also be greater, after a given time, for larger fault throw rates because the knickpoint height from the fault depends directly on the fault throw rate increase, but not on catchment size (Figure 1c) [*Wobus et al*., 2006a; *Whittaker et al*., 2008; *Attal et al*., 2008]. Consequently, a plot of knickpoint height against the throw rate change affecting the channel will form a

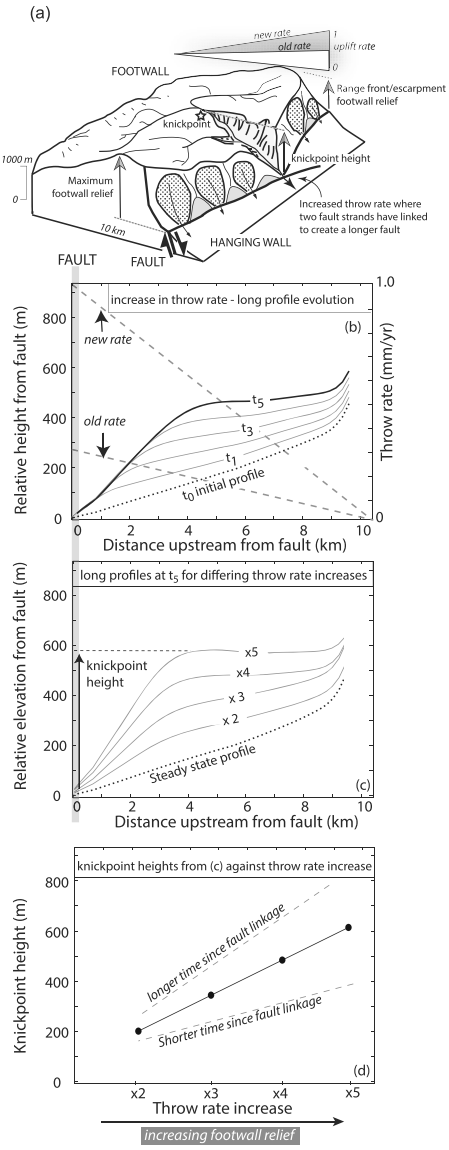

Figure 1. (a) Cartoon showing a footwall catchment responding to an increase in fault throw rate due to fault linkage. The knickpoint represents the farthest extent of a wave of incision that has migrated upstream since the faults linked. Here the relative uplift rate is a maximum at the fault and decays into the footwall. Footwall relief in the uplifting block may be quantified by the maximum elevation difference between the fault and the highest topography along the fault or with respect to a measure of footwall relief. (b) Schematic illustration of a river long profile responding to a threefold increase in fault throw rate, based on field and numerical modeling data [e.g., *Whittaker et al.*, 2008; *Whittaker*, 2012] (Figure 1b) River long profile for a steady state (dotted line) and transient river long profiles for time intervals t_1 to t_5, following fault throw rate increase. (c) Transient river long profiles at t_5, evolved from the same steady state river profile, but for varying throw rate increases. The knickpoint height is measured from the fault to the slope break in the river long profile. The section of channel downstream of the knickpoint and upstream of the fault has adjusted its steepness to balance the new throw rate on the fault. (d) Knickpoint heights plotted against the fault throw rate increase. Knickpoints form a linear trend of increasing height for increasing throw rate difference; the gradient of the line reflects the time since the fault changed its rate.

straight line if the tectonic perturbation was synchronous across the area; the gradient of the line is related to the time since the transient wave of incision started to propagate (Figure 1d).This relationship has been demonstrated for rivers crossing active faults in the Central Apennines [*Whittaker et al.*, 2008]. The height of these knickpoints may also be related to the footwall relief of the fault if an erosionally controlled threshold footwall elevation has not yet been reached [cf., *Densmore et al.*, 2004, 2007]. Finally, while the vertical height of knickpoints should be independent of catchment size, the distance upstream the knickpoints have migrated since their formation should be proportional to the catchment drainage area, *A*. For a simple unit stream power model with uniform rock strength, the rate of retreat should scale as A^m, where m~0.5 [*Tucker and Whipple*, 2002; *Wobus et al.*, 2006b; *Whittaker and Boulton*, 2012].

Nevertheless, most geomorphic studies attempting to derive fault slip rates from long profile analyses have produced qualitative results [e.g., *Boulton and Whittaker*, 2009; *Miller et al.*, 2012]. Partly, this is because it is has been difficult to link geomorphic measurements, however chosen or constrained, to absolute rates of fault motion in the absence of independent geologic constraints [*Wobus et al.*, 2006a; *Miller et al.*, 2012]; partly, it is because even where independent tectonic constraints exist, they typically differ in terms of measurement time scale and/or magnitude. These differences may reflect uncertainties associated with time averaging, but they may also reflect the changing fault slip rates in time and space as a fault array grows and evolves [*Cowie*, 1998a; *Densmore et al.*, 2003; *Boulton and Whittaker*, 2009].

Therefore, an important but underexplored challenge, is to understand how the process of fault growth and interaction itself [*Dawers and Anders*, 1995; *Cowie*, 1998a, 1998b] is expressed in fluvial systems eroding footwall blocks [cf., *Commins et al.*, 2005; *Whittaker et al.*,

2007a; *Boulton and Whittaker*, 2009] (Figure 1a). The fault growth and interaction process ultimately driven by stress feedback between adjacent faults [e.g., *Cowie*, 1998a, 1998b; *Cowie and Roberts*, 2001], and it is now understood to be the mechanism by which an enhancement of slip rates on growing faults takes place over time. This slip rate enhancement, typically on centrally located fault segments within a growing fault array, is due to the loading of these optimally located strands by the failure of neighboring segments along strike. In the absence of a fundamental change in wider tectonic boundary conditions or geodetic rates, it is this phenomenon that rivers record whenever fault slip rate changes are invoked to explain the observations of transient landscapes in areas of active normal faulting [*Cowie et al*., 2006; *Whittaker et al*., 2008]. In fact, it is likely that rivers crossing faults are often subject to increased fault slip rates as individual fault strands grow together and link [cf., *Commins et al*., 2005; *Whittaker et al*., 2007a; *Cowie et al*., 2008; *Hopkins and Dawers*, 2014]. Additionally, it is recognized that interacting faults do not need to be joined (hard linked) for a slip rate enhancement to take place along a fault array [*Cowie*, 1998a; *Cowie and Roberts*, 2001]. Topographic observables such as footwall relief, which reflects (or partially reflects) the growth history of active faults provide one means of identifying the growth and interaction of fault segments [cf., *Densmore et al*., 2004, 2007].

In principle, fluvial landscapes are an ideal tracer for this process, because the time scale over which faults are documented to grow and interact (i.e., 10^5–10^6 years) is similar to recent estimates of landscape response times to a change in fault slip rate at the scale of an individual footwall block [*Cowie and Roberts*, 2001; *Whittaker et al*., 2007a; *Whittaker and Boulton*, 2012]. In this paper we quantify how the growth and interaction of Pliocene to Recent active normal faults in the Sperchios Basin and Northern Gulf of Evia, Greece, are recorded by the landscape. We combine geomorphic analyses including the spatial distribution of footwall relief, knickpoints, and channel steepness with constraints from structural geology and fault interaction theory. We use these data to reconstruct the history of fault linkage along strike of the active faults, deduce their present-day throw rates, and reconcile competing estimates of fault slip rates in time and space.

2. Geological Setting

2.1. Tectonic Setting of Greece

The active tectonic and geodynamic setting of Greece has been widely reviewed [e.g., *Billiris et al*., 1991; *Clarke et al*., 1998; *Davies et al*., 1997; *Hollenstein et al*., 2008; *Roberts and Jackson*, 1991; *Le Pichon and Angelier*, 1979; *Jackson*, 1994], so only a brief summary is given here. Seismicity and active faulting, which are strike slip to extensional in nature, is distributed over a region of an approximately 60,000 km^2 of Greece, western Turkey, Bulgaria, and the Balkans [*Goldsworthy and Jackson*, 2001]. This is generated by the westward motion of Turkey relative to Eurasia, and similar rates of northeast verging subduction along the Hellenic Trench, resulting in N-S extension of the Aegean Sea and normal faulting across mainland Greece [*Goldsworthy et al*., 2002; *Vassilakis et al*., 2011]. Overall, it is one of the most rapidly extending regions on the continents today [*Goldsworthy and Jackson*, 2001; *Roberts and Jackson*, 1991]. Rates of motion are relatively well known from geodetic studies: the extension rate of the whole region is 40–60 mm/yr [*Roberts and Jackson*, 1991] with the southern Aegean moving SW relative to Eurasia at ~30 mm/yr [*Clarke et al*., 1998] and extension across central mainland Greece equaling 10–20 mm/yr [*Clarke et al*., 1998; *Roberts and Jackson*, 1991]. At least 10 mm/yr occurs in the Gulf of Corinth and 1–3 mm/yr in the Gulf of Evia (Figure 2) [*Clarke et al*., 1998; *Goldsworthy et al*., 2002; *Walker et al*., 2010]. Estimates of Holocene slip rates on faults, where derived, are roughly consistent with these rates, but large uncertainties exist [e.g., *Walker et al*., 2010].

2.2. Regional Tectonics of Central Greece

This study focuses on the Northern Gulf of Evia and the Sperchios Basin, central Greece (Figure 2). Faulting in this location has been studied using structural, geodetic, and geomorphological approaches [*Eliet and Gawthorpe*, 1995; *Cundy et al*., 2010; *Walker et al*., 2010], although published estimates of fault slip rates are sparse. The faults have been active since the middle Pliocene (approximately 3.6 Ma) [*Goldsworthy et al*., 2002; *Jackson*, 1999], and there is evidence of linkage of fault segments since they became active [*Goldsworthy et al*., 2002; *Cowie et al*., 2008]. The main set of faults are E-W to ESE-WNW trending normal faults, which have created a series of horsts and half grabens, such as the Gulf of Evia [*Tzanis et al*., 2010; *Eliet and Gawthorpe*, 1995]. The faults extending to depths of 10–15 km are concentrated into subparallel linear zones of discontinuous

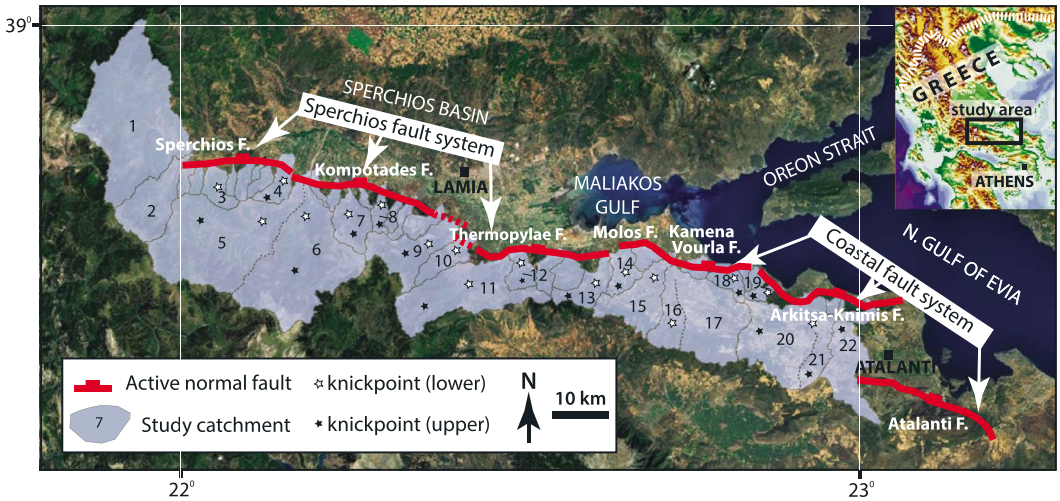

Figure 2. Map of the study area showing the location of the Sperchios Fault system and the Coastal Fault system of the Northern Gulf of Evia, including the Atalanti Fault, (not studied in detail in this study). The inset shows position of study area in relation to Greece. Footwall catchments to the fault system are shaded in blue, and the numbered catchments were selected for study (see Methodology). The major active normal fault strands are shown in red. The upper and lower knickpoints on studied rivers are shown as black and white stars, respectively.

to linked segments a few tens of kilometers long [*Goldsworthy et al.*, 2002; *Goldsworthy and Jackson*, 2001; 2000]. Although the fault zones are not always well defined, especially at their tips, they are clear where faulting produces large topographic relief [*Goldsworthy et al.*, 2002; *Eliet and Gawthorpe*, 1995; *Cowie et al.*, 2008; *Walker et al.*, 2010], exhuming footwall lithologies including Mesozoic limestones and Neogene sediments (Figure 3) [*Roberts and Jackson*, 1991; *Eliet and Gawthorpe*, 1995; *Goldsworthy and Jackson*, 2000].

2.2.1. Northern Gulf of Evia and the Coastal Fault System

The Northern Gulf of Evia is extending at 1–3 mm/yr [*Clarke et al.*, 1998]. We focus on the a series of NE dipping normal fault segments bounding the southern coast of northwest Gulf of Evia [*Cundy et al.*, 2010; *Walker et al.*, 2010] (Figures 2 and 3). These faults are argued to accommodate a significant proportion of the geodetically measured extension across the region [*Walker et al.*, 2010]. The faults uplift Mesozoic limestone and Neogene sediments in their footwalls (Figure 3) [*Goldsworthy and Jackson*, 2001; *Roberts and Jackson*, 1991], and the

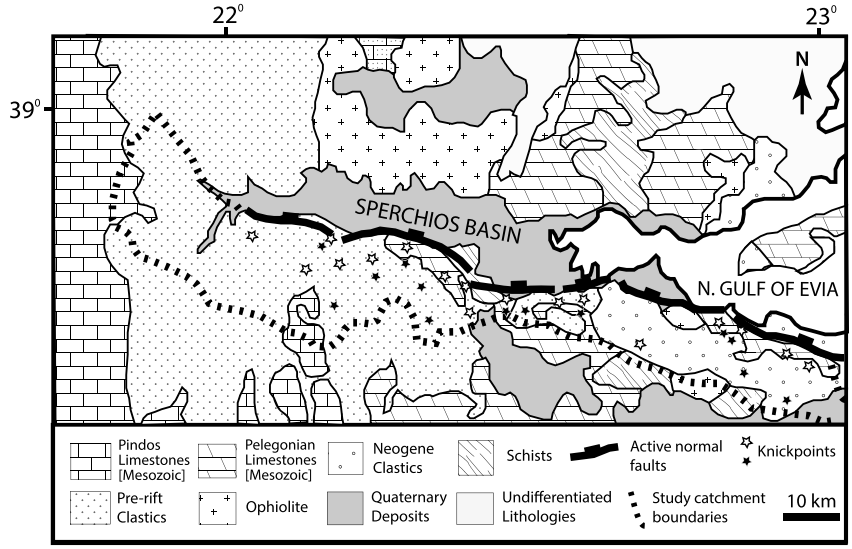

Figure 3. Geological map of the study area showing main lithological units, active normal faults, and study catchment boundary adapted from *Eliet and Gawthorpe* [1995]. The upper and lower knickpoints on studied rivers are shown as black and white stars, respectively. Knickpoints do not coincide with geological contacts.

footwall ridge has relief of up to 1 km. The main fault segments from the NW to the SE are the Molos-Kamena Vourla, Knimis-Arkitsa, and Atalanti normal faults, usually referred to as the Coastal Fault system [*Walker et al*., 2010; *Cowie et al*., 2008; *Cundy et al*., 2010]. We focus on the Molos-Kamena Vourla and Knimis-Arkitsa Fault segments in this paper. The Atalanti Fault, not studied in detail here, is the easternmost structure which is approximately 35 km long with a throw rate up to 1.6 mm/yr based on paleoseismological trenching [*Pantosti et al*., 2004]. It ruptured twice in 1894, with estimated moment magnitudes of 6.8. In contrast, there are no large earthquakes documented on the other fault segments in the last 300 years [*Pantosti et al*., 2004].

The Arkitsa-Knimis Fault, is an E-W striking, north dipping fault, located to the SE of the Kamena Vourla Fault and NE of the Atalanti Fault, which formed due to the linkage between the previously separated Knimis and Arkitsa Fault segments [*Walker et al*., 2010] (Figure 2). Estimates of fault linkage time are uncertain, but Pleistocene sediments uplifted in the breached relay zone suggest that this event occurred at around 1 Ma [*Cowie et al*., 2008]. The Knimis Mountain contains Mesozoic limestones and Plio-Pleistocene sediments at elevations of up to 800 m. The minimum throw of the Arkitsa Fault segment is estimated to be at least 600 m, based on the thickness of Neogene-Holocene sediments in the hanging wall plus the scarp height and topographic relief of the footwall block [*Jones et al*., 2010], while the Knimis Fault segment has a footwall component of throw >900 m, based on outcropping early Pliocene Karya formation on top of Mount Knimis [*Kranis*, 2007]. Seismic profiles reveal 300–400 m of sediment thickening into this structure, suggesting a total throw of >1400 m [*Sakellariou et al*., 2007]. While this fault is acknowledged to be active, there is little consensus regarding Holocene and late Pleistocene fault slip rates [cf., *Cundy et al*., 2010]. The Pleistocene sediments uplifted in the breached relay zone between the Arkitsa and Knimis Fault segments are consistent with time-averaged throw rates of 0.3–0.5 mm/yr in this locality over 1 Ma [*Cowie et al*., 2008]. Toward the NW end of the Knimis Fault, terraces of the Voagris River, attributed (but not dated) to marine oxygen isotope stag 5e, would suggest a throw rate of <0.2 mm/yr [*Goldsworthy and Jackson*, 2001], while toward the eastern end of the Arkitsa Fault segment near the village Kynos, a vertical uplift rate of ~0.2 mm/yr, relative to sea level, is also estimated based on coastal notches [*Pirazzoli et al*., 1999; *Goldsworthy and Jackson*, 2001; *Walker et al*., 2010]. In contrast, <5 km to the east of the *Cowie et al*.'s [2008] study site, *Cundy et al*. [2010] estimate late Holocene uplift rates on the Arkitsa Fault near Alope of ~1 mm/yr from coastal geomorphology, fossil, and historical artifact constraints, implying vertical uplift rates at least as large as the slip rate of the Atalanti Fault. The differences between these rates conflate uncertainties in the age of offset deposits, the time scale over which the rates are averaged, and the expected variation in fault slip rates along strike of major structures.

The Kamena Vourla and Molos Fault segments are E-W striking 30 km long faults, which dip at 50°N [*Goldsworthy and Jackson*, 2001; *Walker et al*., 2010]. Footwall lithologies are Mesozoic limestone and Neogene sediments, with minor outcrops of mafic ophiolitic rocks and deep-sea cherts [*Roberts and Jackson*, 1991; *Walker et al*., 2010] (Figure 3). The throw rate along this part of the fault system is not well known, but based on river terraces at the footwall-hanging wall transition close to the town of Molos, *Walker et al*. [2010] estimate an approximately 1 mm/yr vertical component of slip. However, these rates have significant error bars because the actual age of the terraces was not well resolved using either optically stimulated luminescence or ^{14}C dating techniques. If correct, the terrace offset would translate to a Holocene rate of extension across the fault of 0.6–1.7 mm/yr assuming 30°–60° fault dip [*Walker et al*., 2010].

2.2.2. The Sperchios Fault System

The Sperchios Basin is the most northerly of the central Greece rift basins at the northwest end of the Gulf of Evia (Figure 2). It is a 100 km long and 30 km wide asymmetric half-graben basin, thought to have been active by 3.6 Ma and throughout the Pleistocene [*Eliet and Gawthorpe*, 1995; *Roberts and Ganas*, 2000; *Walker et al*., 2010]. The fault is made up of three major fault segments [*Eliet and Gawthorpe*, 1995; *Goldsworthy and Jackson*, 2001], which attain a topographic relief of 1000–2000 m; these are the Sperchios, Kompotades, and Thermopylae (Lamia) segments (Figure 2). They are morphologically similar to the Coastal Fault system, of which it is argued to be the western continuation and potentially kinematically linked [*Goldsworthy et al*., 2002; *Walker et al*., 2010]. The topographic relief, coupled with gravity studies that indicate >2.5 km of Pleistocene sediment in the basin, suggests a total throw on the basin bounding fault of ~4 km [*Eliet and Gawthorpe*, 1995]. Constraints on the throw rate of the Sperchios Fault system are sparse. *Eliet and Gawthorpe* [1996] suggest rates of up to 2.4 mm/yr based on limited seismic data from the Maliakos Gulf, while the estimated total throw of ~4 km would suggest a lower long-term rate of 1.1 mm/yr in the center of the fault system, assuming that displacement had commenced by 3.6 Ma as the sedimentary basin fill suggests.

3. Methodology and Approach

A merged DEM of the study area (UTM zone 34 N) was created using a set of 30 m Advanced Spaceborne Thermal Emission and Reflection Radiometer DEM tiles of central Greece. A stream network was derived in ArcGIS with a threshold initiation drainage area of 0.27 km^2 (i.e., 300 pixels), and we digitized the locations of active faults using information from literature (section 2), their geomorphic expression on Google Earth, and DEM topography. Study catchments that drain the footwall blocks of the Sperchios and Coastal Fault systems were selected with drainage areas > 5 km^2 and catchment lengths > 5 km at the fault. This was to ensure that we only analyzed fluvially dominated channels, and in total, 22 of the footwall catchments met these criteria (Figure 2). From our DEM, fault map, and stream network, we made a number of geomorphic and topographic measurements, summarized in Tables 1 and 2. A key variable we wished to constrain was the footwall relief of the fault systems (cf., Figure 1a). Because there are different ways of measuring this variable on a catchment or range scale [e.g., *Densmore et al*., 2007; *D'Arcy and Whittaker*, 2014], we adopted two complementary methods to determine this. In the first method, we took 44 individual topographic profiles, measured perpendicular to the faults, along strike of the two fault systems (Tables 1 and 2 and Figure 4). We used these to determine the distribution of footwall relief along strike, here defined as the absolute change in elevation from the fault to the crest of the uplifted footwall. For these profiles, the crest of the uplifted footwall was taken as the position of the first major topographic break in slope in the footwall, which corresponded to the top of the prominent triangular facets present in some localities and hence can be taken to be equivalent to the range front relief. Identical profiles, measured along strike of the fault within ±200 m of the original profile suggested that the error associated with this footwall relief measurement is ±10%. The position of the fault in the topographic profile corresponded to its position as traced in ArcMap. In the second method, we defined two polygons containing all the topography clearly associated with the two active fault systems in ArcGIS (Figure 4), and we used the focal statistics tools to determine the maximum elevation of the raster data within each polygon in a swath profile projected parallel to the fault strike. From this, we subtracted the elevation of the proximal hanging wall along strike to obtain the relief. For this study area, defining "footwall relief" based on the maximum and minimum elevations of individual catchments draining the footwall [cf., *Densmore et al*., 2004; *D'Arcy and Whittaker*, 2014] is not appropriate, because a number of catchments flow parallel to the fault, complicating the relationship between relief and along-strike position, and because some of the larger catchments toward the tips of faults impinge on topography that is related to other structures. The two methods of determining relief produce consistent results, with the second method yielding higher footwall relief. The footwall relief, derived using the methods above, was subsequently compared to the location and segment lengths of the digitized faults (Figure 4).

Second, MATLAB and ArcGIS were used to extract stream longitudinal profiles to create a data matrix including upstream distance, elevation, channel gradient, drainage area, and geographic coordinates for each of the studied rivers using a smoothing window of 100–250 m and a contour resampling interval of 10 m. From the long profiles (Figure 5), we documented the presence of knickpoints upstream of the active faults, measured to the slope break in the long profile [*Wobus et al*., 2006a; *Whittaker and Boulton*, 2012]. While the term "knickpoint" is sometimes used to describe discrete or small-scale features such as waterfalls, in this paper we focus on steep reaches upstream of active faults (knickzones), which create a local convexity in what would otherwise be a concave-up river long profile. The knickpoint itself is defined here as the precise point in the smoothed long profile where the rate of change of channel gradient reaches a local maximum; this was verified by comparison with derived slope-area plots [cf., *Wobus et al*., 2006a]. Knickpoint locations are shown with stars in Figure 5, and relevant knickpoint data are documented in Tables 1 and 2. Where present, we measured the vertical height of the knickpoint, relative to the basin-bounding fault, following the methodology of *Whittaker and Boulton* [2012]. Additionally, we computed normalized steepness indices, k_{sn}, (equation (2)) for the study rivers using a reference concavity of 0.45 [*Wobus et al*., 2006a]. Where present, these were calculated for river reaches upstream and downstream of knickpoints.

From these data, we compared the distribution of knickpoint heights and channel steepness along strike of the studied faults with the measured footwall relief and with existing constraints on fault throw, throw rate, and independent measurements of footwall uplift rate relative to sea level from stratigraphic and geomorphic constraints (section 2). These data were used to evaluate the extent to which geomorphic metrics recorded the Pliocene to recent history of fault growth and interaction of the Sperchios and Coastal Fault systems.

Table 1. Data for Sperchios Fault System

Distance Along Fault Strike (m)	Topographic Profile	Stream Number	Footwall Relief[a] (m)	Fault Elevation (m)	Drainage Area (km^2)	Presence of Knickpoint?[b]	Knickpoint Height From Fault (m)	Knickpoint Upstream Position From Fault (m)	k_{sn} Below Knickpoint ($m^{0.9}$)	k_{sn} Above Knickpoint ($m^{0.9}$)
−180		1	*100*	257	182.8	0			110	
0	A		280							
213	B		584							
1,522		2		313	49.1	0			117	
3,953	C		552							
5,857		3	*599*	359	10.8	1	314	2,516	121	64
5,866	D		636							
8,627	E		814							
11,072	F		1,002							
14,046	G		796							
16,485		4	*790*	186	12.2	2	794	6,735	106	34
16,485		4	*790*	186	12.2	1	335	4,444	239	106
16,951	H		490							
19,186	I		163							
20,988		5	*800*	176	291.4	2	444	21,576	72	52
20,988		5	*800*	176	291.4	1	256	10,723	130	72
20,988		6	*800*	176	291.4	2	716	14,760	90	47
20,988		6	*800*	176	291.4	1	216	8,738	140	90
21,161	J		1,190							
23,774	K		1,228							
25,107		7	*1,100*	309	26.7	2	1,394	8,436	190	45
25,107		7	*1,100*	309	26.7	1	634	3,797	248	190
26,471	L		1,017							
28,855	M		1,488							
29,147		8	*1,470*	326	7.9	2	1,471	5,560	135	31
29,147		8	*1,470*	326	7.9	1	827	2,341	406	135
31,669	N		1,466							
34,201	O		1,374							
36,483	P		1,200							
40,266	Q		1,277							
40,582		9	*1,270*	227	43.9	2	1,294	7,982	165	43
40,582		9	*1,270*	227	43.9	1	893	2,853	557	165
43,449	R		464							
44,256		10	*460*	140	18.5	1	610	3,591	248	96
46,680	S		393							
48,513		11	*500*	78	86.1	2	872	1,3228	172	74
48,513		11	*500*	78	86.1	1	457	6,069	179	172
49,433	T		759							
51,616	U		921							
53,547	V		988							
55,626		12	*1,050*	51	7.4	2	835	4,038	227	42
55,626		12	*1,050*	51	7.4	1	457	2,466	197	227
56,013	W		1,264							
58,270	X		986							
60,507	Y		754							
64,838		13	*350*	202	16.8	2	791	6,779	137	28
64,538		13	*350*	202	16.8	1	341	2,454	155	137
65,218	Z		37							

[a]Footwall relief in italics for streams are interpolated between along strike measurements as appropriate.
[b]Presence of knickpoint: 0 = no knickpoint, 1 = lowermost or single knickpoint, and 2 = uppermost of two knickpoints.

4. Results

4.1. Footwall Relief and Fault Segmentation

Fault position and footwall relief along strike is shown for the Sperchios and Coastal Fault zones in Figure 4, along with existing tectonic constraints from section 2. For the Sperchios Fault system, the maximum footwall relief from the swath profile parallel to the fault reaches values of ~2000 m at around 30 km along strike from

Table 2. Data for Coastal Fault System

Distance Along Fault Strike (m)	Topographic Profile	Stream Number	Footwall Relief[a] (m)	Max Footwall Relief	Fault Elevation (m)	Drainage Area (km^2)	Presence of Knickpoint?[b]	Knickpoint Elevation (m)	Knickpoint Height From Fault (m)	Knickpoint Upstream Position From Fault (m)	k_{sn} Below Knickpoint ($m^{0.9}$)	k_{sn} Above Knickpoint ($m^{0.9}$)
0	a		100									
1,050		14	*150*	*400*	46	18.4	2	480	434	7,017	68	17
1,050		14	*150*	*400*	46	18.4	1	337	291	5,200	52	68
1,376	b		154									
3,614	c		228									
4,662		15	*200*	*200*	56	45.3	1	109	53	3,004	75	118
6,143		16	*100*	300	56	104.2	1	308	264	7,939	72	49
6,417		17	*100*	100	56	104.2	0				50	
6,417	d		49									
8,547	e		327									
10,913	f		592									
13,444	g		845									
14,100		18	*750*	800	38	6.2	2	773	735	4,159	56	14
14,100		18	*750*	*800*	38	6.2	1	531	493	1,616	275	56
15,696	h		834									
18,463	i		621									
19,952		19	*620*	*720*	145	3.1	2	700	555	2,719	54	27
19,952		19	*620*	*720*	145	3.1	1	514	369	814	344	54
21,565	j		621									
23,700	k		332									
25,323	l		276									
25,457		20	*320*	*370*	50	101.4	2	446	396	17,068	45	18
25,457		20	*320*	*370*	50	101.4	1	145	95	3,782	95	45
25,457		21	*320*	*370*	50	101.4	2	258	208	9,238	38	35
25,457		21	*320*	*370*	50	101.4	1	145	95	3,782	95	38
27,636	m		630									
29,965	n		573									
32,783	o		423									
34,815		22	*270*	*500*	62	5.6	2	443	381	4,159	53	18
34,815		22	*270*	*500*	62	5.6	1	208	146	747	122	53
35,369	p		241									
37,785	q		202									
40,550	r		100									

[a]Footwall relief in italics for streams are interpolated between along strike measurements as appropriate.
[b]Presence of knickpoint: 0 = no knickpoint, 1 = lowermost or single knickpoint, and 2 = uppermost of two knickpoints.

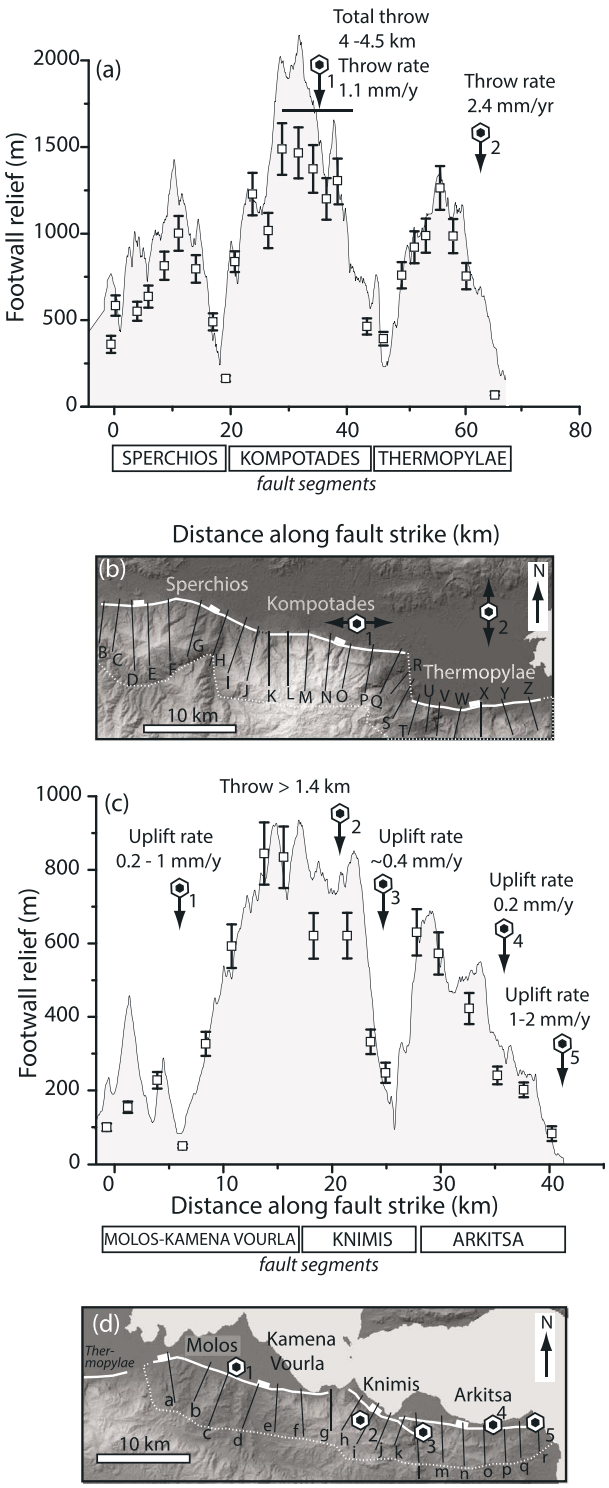

Figure 4

east to west (i.e., at the center of the fault) and declines in both directions toward the tips of the fault system (Figure 4a). An almost identical trend is observed for footwall relief measurements based on individual topographic profiles measured perpendicular to the strike of the fault (Figure 4b), suggesting that our measurements of footwall relief are robust and consistent. To the first order, the pattern of footwall relief seen here is expected for fault strands interacting and behaving as a single system, where the footwall relief is reflecting greater throw (i.e., the vertical component of displacement) in the center of the fault system, and limited tectonically controlled topography at the tips [*Cowie and Roberts*, 2001; *Densmore et al*., 2007; *Boulton and Whittaker*, 2009]. However, there are three well-defined maxima in footwall relief, which clearly correspond to the locations of the individual mapped fault segments—the Sperchios, Kompotades, and Thermopylae segments, respectively (Figure 4b). These segments have mapped lengths of ~20 km each [*Eliet and Gawthorpe*, 1995] and are separated by two substantial minima in footwall relief of 200–400 m. This observation strongly suggests that the fault system has grown by the interaction and linkage of these three fault strands [*Cowie*, 1998a; *Cowie and Roberts*, 2001; *Goldsworthy et al*., 2002], with substantially higher footwall relief now having been generated in the footwall of the Kompotades segment of the Sperchios Fault system compared to the Sperchios and Thermopylae segments.

The close correlation between the fault strands and the footwall relief variation along strike shown in Figure 4a raises the question of the extent to which footwall topography reflects the underlying variation in the throw along the fault. Footwall relief can become decoupled from fault displacement toward the center of a fault if a (erosionally limited) threshold elevation is reached, while continuing to record fault displacement variation at the fault tips [*Densmore et al*., 2004, 2007]. Here the good correlation between the footwall relief and the fault segmentation pattern, with little evidence of a "plateau" in relief along strike, suggests that variations in fault throw are generally being recorded in footwall relief, in circumstances where individual segments are ~20 km long and the total fault length is ~60 km. The estimated total throw

of 4–4.5 km in the center of the fault [*Eliet and Gawthorpe*, 1995] is a factor of 2–3 times larger than the footwall relief. This factor is consistent with that derived from other faults of similar size in previous studies [e.g., *Mirabella et al*., 2004]. However, measures of throw rate along strike (Figures 4a and 4b, hexagons) show less consistency; this may reflect the differing assumptions and time spans used to estimate these values, and we return to this issue in the discussion.

For the Coastal Fault system, the maximum footwall relief reaches values of ~950 m (Figure 4c), approximately half of the relief of the Sperchios system, and declines to low values toward both tips of the fault. Again, there is a good match between our two methods of estimating footwall relief, indicating that our results are reliable and consistent. Shorter length scale maxima correspond to the location of the Arkitsa, Kamena-Vourla-Knimis, and Molos Fault segments, while two minima in footwall relief separate these individual mapped fault segments, which have mapped lengths of approximately 10 km (Figure 4d). These fault segments are known to be physically linked in the case of the Arkisa-Knimis strands, where the old relay ramp at the Logos Fan (location 3) is breached [cf., *Cowie et al*., 2008], while the boundary between the Knimis and Kamena-Vourla faults is not distinguishable in terms of relief. Like the Sperchios system above, the close correspondence between fault segmentation and topography over length scales < 50 km suggests that variations in footwall relief do reflect variations in throw along strike of this fault system.

Where independent estimates of total throw are available for the Coastal Fault system (e.g., location 2, Figure 4b, from *Sakellariou et al*. [2007]), footwall relief is 40–55% of this value. This indicates that the total throw on the fault is a factor of 2–2.5 times greater than the measured footwall relief. This is consistent with previous studies on normal faults of this size [*Mirabella et al*., 2004; *Whittaker et al*., 2007b]. Consequently, we estimate that the total throw at the center of the Kamena Vourla segment lies between 1700 m and 2300 m. For the two fault systems, the ratio of the maximum footwall relief to the total length of the fault system is 0.02–0.03, giving identical scaling between fault size and fault throw for the two systems [*Cowie and Roberts*, 2001]. Finally, it is noticeable that footwall relief does not quite fall to zero where the Thermopylae segment of the Sperchios Fault zone meets the Molos Fault segment of the Coastal Fault system. This suggests that these two fault systems themselves are beginning to interact [cf., *Walker et al*., 2010].

4.2. River Long Profiles and Knickpoint Heights

In general, these channels crossing the Sperchios and Coastal Fault systems do not have concave-up profiles consistent with steady state landscapes, but rather show convex long profiles with one or typically two knickpoints upstream of the fault (Figure 5). A general trend is present for both fault zones, where the rivers at fault tips have no knickpoints (e.g., rivers 1, 2, 5, or 17), while many channels located toward the centers of the

Figure 4. (a) Footwall relief along strike of the Sperchios Fault system, with the three main fault strands marked. (b) DEM hillshade image of the Sperchios Fault system showing spatial location of fault strands, throw constraints, and swath cross sections (letters are coded to the relief measurements in Table 1). The white dotted line contains the polygon used to derive maximum topographic relief in Figure 4a from a single swath profile along strike of the fault. (c) Footwall relief along strike of the Coastal Fault system, with the main fault strands marked. The squares and the grey profile depict the same as in Figure 4a but for the Coastal Fault. The black and white hexagons show existing estimates on the throw and/or throw rate of the fault strands from *Pirazzoli et al*. [1999], *Goldsworthy and Jackson* [2001], *Sakellariou et al*. [2007], *Cowie et al*. [2008], *Cundy et al*. [2010], and *Walker et al*. [2010] as summarized in section 2.2.1. (d) DEM hillshade image of the Coastal Fault system showing spatial location of fault strands, throw constraints, and swath cross sections (letters are coded to the relief measurements in Table 2). The white dotted line contains the polygon used to derive maximum topographic relief in Figure 4c from a single swath profile the strike of the fault. The grey profile in Figure 4a represents maximum topographic relief along strike, extracted from the polygon in Figure 4b, containing all relief associated with footwall of the fault. The squares correspond to the elevation difference between the fault and the first major break in slope for each of the individual topographic profiles in Figure 4b, representing the range front relief. The error bars represent the difference in footwall relief when the same profiles are moved by ±200 m along strike. The black and white hexagons show the existing estimates on the throw and/or throw rate of the fault from *Eliet and Gawthorpe* [1995] and *Eliet and Gawthorpe* [1996], as summarized in section 2.2.2.

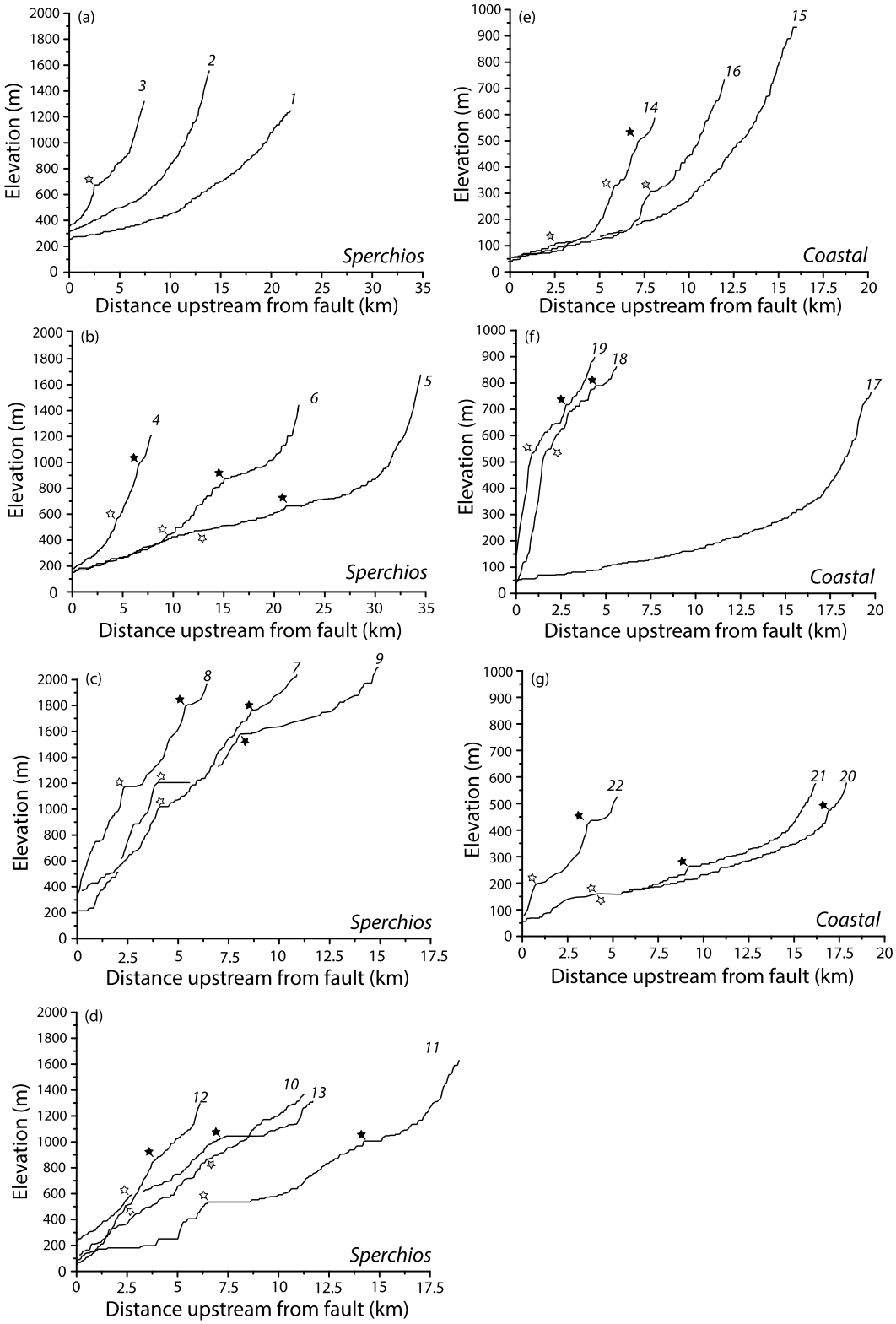

Figure 5. (a–d) Long profiles of rivers crossing faults in the Sperchios Fault system. (e–g) Long profiles of rivers crossing faults in the Coastal Fault system. The numbers correspond to the catchments shown in Figure 2. The white and black stars show the locations of the lower and upper knickpoints upstream of the faults, respectively. The grey stars indicate the rivers where only one knickpoint is identified.

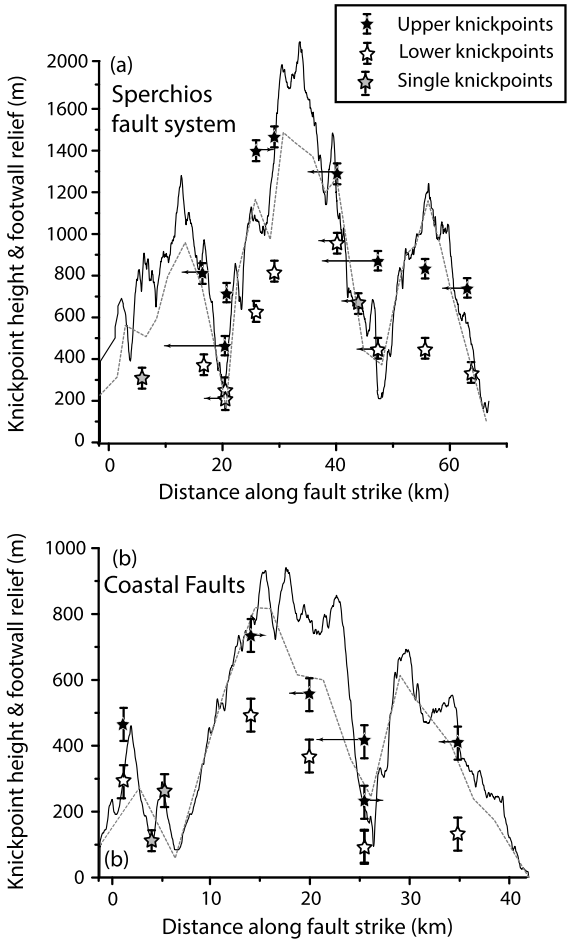

Figure 6. Knickpoint heights on rivers crossing the active faults for (a) the Sperchios and (b) the Coastal Fault systems measured from the active fault. Along strike position of the knickpoint is plotted where the river crosses the fault. The upper set of knickpoints are shown as black stars, and the lower set of knickpoints are shown as white stars. The grey stars show rivers with one knickpoint. The error bars indicate the ±50 m uncertainty in the height of the knickpoint which reflects our estimate of the precision of fault locations and knickpoint positions on the DEM. The arrows indicate where knickpoint is located along strike of the fault if this is different from the fault-river crossing position. The thin black line shows maximum footwall relief along strike for each fault system, derived from the strike-parallel swaths shown in Figure 4, and plotted on the same vertical scale. The grey dotted line shows the envelope of range footwall relief values interpolated from individual strike-perpendicular topographic profiles for each fault system.

two fault zones and in positions where fault segments are linked show one or often two knickpoints in long profile (e.g., rivers 9 and 11; cf., Tables 1 and 2). The interpretation that the knickpoints are due to lithological differences is ruled out because they do not systematically correlate with lithological boundaries in the study areas (Figure 3). Instead, these stream long profile shapes are consistent with a transient response of the fluvial network to active faulting [*Whittaker et al*., 2008; *Boulton and Whittaker*, 2009; *Miller et al*., 2012; *Cowie et al*., 2008].

The close relationship between the active faults and the presence and size of knickpoints becomes obvious if we consider the height of knickpoints, measured vertically upstream from the active fault, and plotted along strike of the two systems, where the river on which they are located crosses the fault. For the Sperchios Basin (Figure 6a), rivers at the western end of the fault have no knickpoints (Figure 5, rivers 1 and 2, and Table 1), while in the center of the fault, there are upper and lower knickpoint pairs on most rivers. Significantly, the upper knickpoints (black stars) are at a similar height as the footwall relief of the fault (where a knickpoint appears slightly higher than the footwall relief, this is because the river on which it lies does not flow perpendicular to the fault). The lower set of knickpoints (white stars) also increase in height toward the center of the fault and form a triangular pattern with a decline in relative elevation toward the fault tips, albeit at a lower absolute height.

Similar observations can be made in the Coastal Fault zone, where again, the upper set of knickpoints mirror the footwall relief, particularly so for the relief envelope produced from our strike-perpendicular profiles (Figure 6b, dashed line). The lower set of knickpoints shows a similar trend, with greatest heights near the center of the fault but at a consistently lower height measured relative to the fault. Where the Sperchios and Coastal Fault systems (Figure 4d) meet, we also see paired knickpoints and some single knickpoints upstream of the Molos Fault strand.

We test the relationship between the knickpoints and faulting explicitly by plotting knickpoint heights against the footwall relief for each channel (Figure 7). We choose to use maximum footwall relief for this exercise as we have greater data coverage along strike, but the results are similar using the strike-perpendicular measure of footwall relief. For both fault systems, the data can be fitted with a simple linear relationship between knickpoint height and footwall relief. For the upper knickpoints, knickpoint height is on average 86% of the maximum footwall relief in both fault systems. For the lower knickpoints,

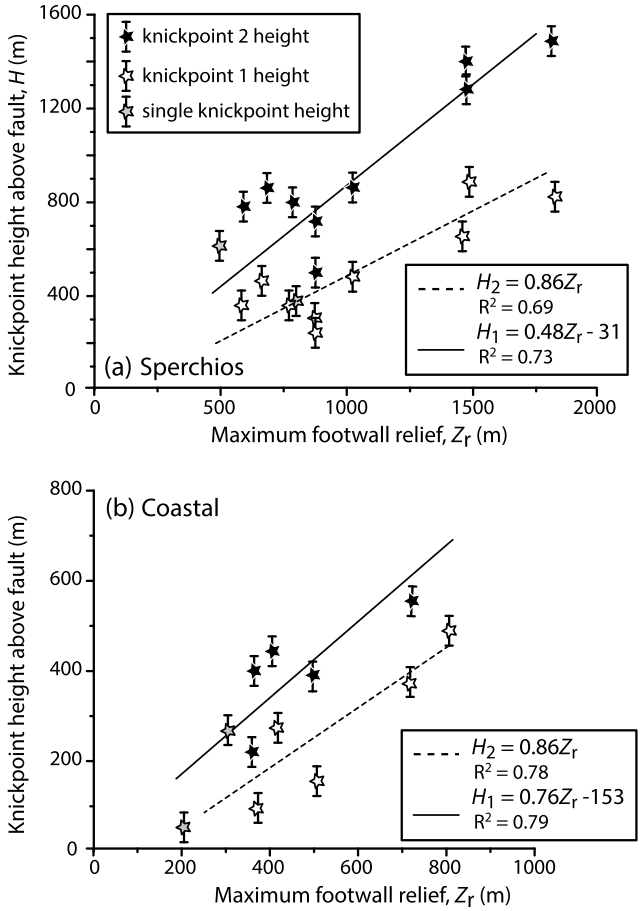

Figure 7. Knickpoint height, measured from the bounding fault, against maximum footwall relief for (a) the Sperchios and (b) the Coastal Fault systems. The error bars are identical to Figure 6. For simplicity, the maximum footwall relief is derived from where the river containing the knickpoint crosses the fault along strike. The black stars show the upper knickpoint heights, and the white stars show the lower knickpoint heights. Rivers with only a single knickpoint are shown in grey. The solid line shows a simple linear fit through the upper knickpoint heights. The dashed line shows a simple linear fit to the lower knickpoint heights with their relevant equations and r^2 values.

the best fits are linear with a gradient of 0.45–0.5 and an *x* intercept of 30–150 m, suggesting that some footwall relief before these knickpoints were generated. This relationship between footwall relief and knickpoint heights is similar in form to relationships recently documented in other field sites such as the Italian Apennines, Turkey, and Papua New Guinea [*Boulton and Whittaker*, 2009; *Miller et al.*, 2012; *Whittaker and Boulton*, 2012].

As footwall relief at the scale of these two fault systems is tectonically controlled and records fault segmentation and likely displacement variation along strike (Figure 4), these data point to an explicit link between the history of faulting and the development of the knickpoints. From this perspective, the presence of two knickpoints in most of the long profiles is potentially explained by two perturbations to the tectonic boundary conditions governing the evolution of these channels, which would have to have occurred within the response time scale of the fluvial system [*Miller et al.*, 2012; *Whittaker and Boulton*, 2012].

4.3. Normalized Steepness Indices

Rivers in the study area can generally be divided into three reaches: (i) a lower reach, upstream of the active fault and downstream of the lower knickpoint; (ii) a middle reach, between the two knickpoints, and (iii) an upper reach, consisting of the headwaters upstream of the top knickpoint if present (Figure 8, inset). Normalized steepness indices (k_{sn}) calculated for each of these three reaches show consistent patterns for the two fault systems. Parameter k_{sn} for the upper reaches (grey triangles) is consistently low, reaching a maximum of 50–70 $m^{0.9}$ for rivers draining across the Sperchios Fault (Figure 8a). For the Coastal Fault, the average value for the upper reaches is 40 $m^{0.9}$ (Figure 8b); there is little along-strike variation in both cases. Between the knickpoints, reach-averaged k_{sn} is a maximum of 180–200 $m^{0.9}$ for the central parts of the Kompotades and Thermopylae segments of the Sperchios system, with lower values toward the fault tips. Maximum values of 60 $m^{0.9}$ are recorded along strike of the Coastal Fault system between the knickpoints. In contrast, upstream of the active fault and downstream of the lower knickpoints, k_{sn} vary significantly along strike in both cases: reach-averaged k_{sn} achieves a maximum of 557 $m^{0.9}$ toward the center of Sperchios Fault system and 344 $m^{0.9}$ for the Coastal Fault system before falling toward the tips. These results demonstrate that (i) there is a systematic increase in k_{sn} from the upper to middle and lower reaches for all of the rivers in the study area, (ii) this trend is amplified in the along-strike center of the two faults, and (iii) rivers crossing the Sperchios Fault system have k_{sn} values in the center of the fault that are 1.5–3 times those in the center of the Coastal Fault system.

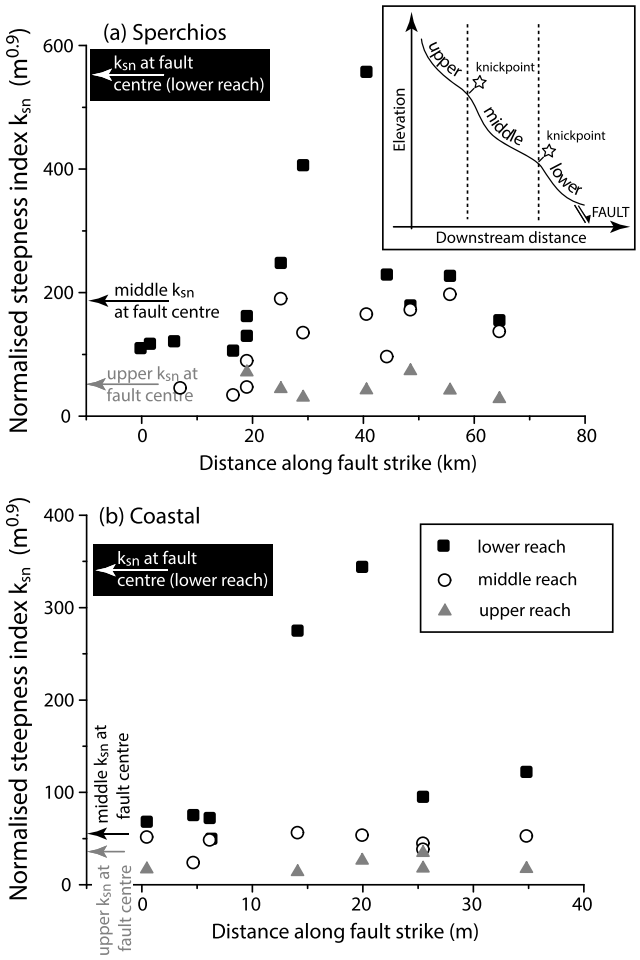

Figure 8. Normalized steepness indices, k_{sn}, for the upper (grey triangles), middle (circles), and lower (black squares) reaches of rivers crossing (a) the Sperchios and (b) the Coastal Fault systems. The inset shows how the upper, lower, and middle reaches of the channels studied relate to the fault and knickpoint positions defined in this paper. The arrows show the normalized steepness indices for the three reaches, as measured in the center of the faults.

5. Discussion

5.1. Fault Relief, Fault Linkage, and Landscape Response

The results above show that for these upper Pliocene to recent fault systems, which are 40–60 km long and have segment lengths < 20 km, tectonically generated footwall relief reflects the history of fault growth and interaction of the fault strands making up the large-scale fault system [cf., *Goldsworthy et al.*, 2002]. The presence of two sets of knickpoints on most of the channels, which are not related to lithology, indicates that these channels have been subjected to at least two changes in base level along the fault, which must have happened within the response time of the fluvial system. The most convincing and consistent explanation for these knickpoints is that they reflect landscape response to fault growth and interaction. The upper set of knickpoints for both fault systems have heights that closely match the footwall relief and scale in a similar way to each other (Figure 7). We know from theory and modeling evidence that the vertical height of knickpoints in a landscape should scale explicitly with both fault throw and throw rate if they are initiated together (Figure 1) [*Whittaker et al.*, 2008; *Boulton and Whittaker*, 2009]. So given that the footwall relief for these fault systems does appear to reflect the history of faulting, we propose that the upper set of knickpoints grew as fault-bounded topography grew, and hence, the knickpoints are recording the accumulation of footwall relief as they have propagated vertically through the landscape since fault initiation [*Wobus et al.*, 2006b]. Other explanations for the upper sets of knickpoints require ad hoc explanation—we have excluded lithology, while other relative base level changes, for instance driven by eustasy, are of smaller magnitude and would not produce knickpoint heights that vary systematically along strike of the faults.

In contrast, while the height of the lower set of knickpoints is also a linear function of the footwall relief, the gradient of the line is lower. These knickpoints are clearly younger than the upper set, and the footwalls had clearly developed some topographic relief prior to these features forming. The simplest way to interpret these knickpoints is that they initiated from a fault linkage event on each fault system, respectively. A good candidate would be when the individual segments of each of the two fault zones started to interact with each set of fault segments kinematically linked as a single structure. This type of fault interaction increases fault throw rates because of repeated stress loading of the centrally located fault segments by failure of neighboring segments located along strike [*Cowie*, 1998a, 1998b]. Additionally, central fault segments are post physical linkage, relatively underdisplaced for the larger fault structure that they become part of, while larger displacement events can occur on longer structures, maintaining higher slip rates [*Dawers and Anders*,

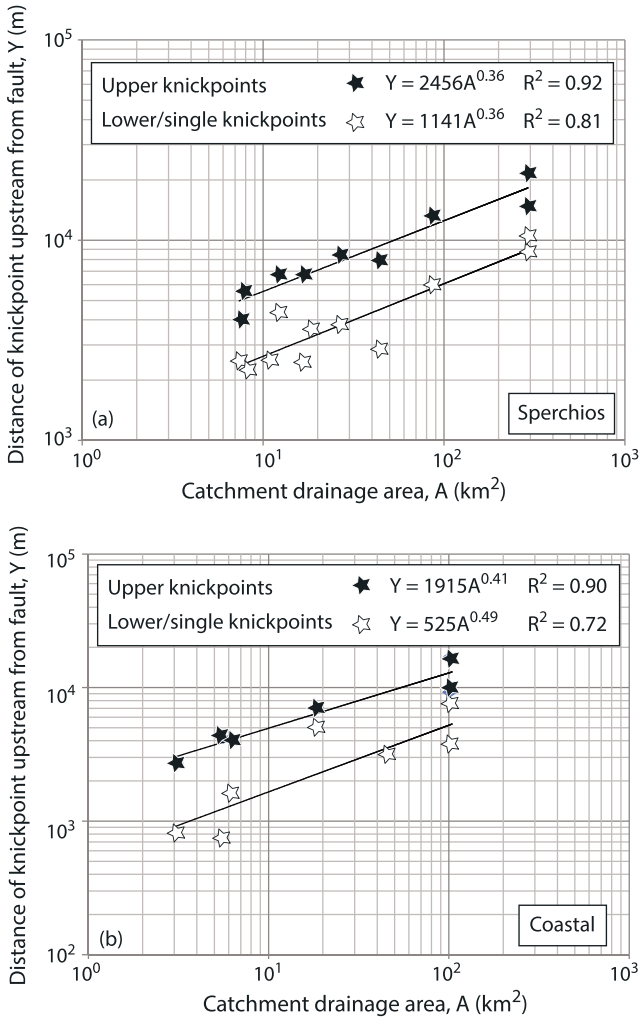

Figure 9. Distances knickpoints have migrated upstream, in plain view, measured from the fault against catchment drainage area for (a) the Sperchios Fault system and (b) the Coastal Fault system. The black stars show the upper knickpoints, and the white stars show the lower (or single) single knickpoints on study rivers. Data are fitted with a power law.

1995; *Cowie and Roberts*, 2001]. Although it has not been widely explored, the slip rate increase resulting from stress reloading feedback probably starts in the early stages of interaction (prior to physical linkage) and may occur rapidly [*Cowie and Roberts*, 2001; *Hopkins and Dawers*, 2014; N. H. Dawers, personal communication].

We are not persuaded that there have been numerous changes in fault slip rates or multiple linkage events along each of the faults at a number of different times because this (i) would not produce the consistent relationships between knickpoint heights and footwall relief documented here and (ii) does not fit the spatial pattern of knickpoints along strike observed in Figure 6. Instead, if our interpretation is correct, knickpoints in rivers with greater drainage areas should have traveled farther upstream in a predictable way, because they would have initiated at the same time [*Wobus et al.*, 2006b; *Whittaker and Boulton*, 2012]. To test this, we plot knickpoint distances upstream against drainage area for the Sperchios and Coastal Fault systems (Figure 9). In both cases, we find that knickpoints have indeed migrated farther upstream where the drainage area is greater. The power law exponent on drainage area lies in the range of 0.36–0.49. This is similar to the exponent of approximately 0.5 that would be predicted for knickpoint celerity using a very simple specific stream power model (section 1) [*Tucker and Whipple*, 2002; *Whittaker and Boulton*, 2012]. For both the Sperchios and the Coastal Fault systems, the coefficient on the power law relationship is similar. Thus, catchments with drainage areas of 10 km^2 have knickpoints that lie at ~5 km upstream from the fault in both cases. These data therefore suggest that the upper sets of knickpoints likely formed at the same time as each other, which is what we would expect if they relate to fault segment initiation. In contrast, the lower set of knickpoints on the Coastal Fault system generally have not migrated upstream as far as in the Sperchios system, so we infer that the fault interaction event that created these knickpoints happened more recently on the Coastal Fault.

5.2. Estimating Fault Throw Rates and Linkage Times

Figure 8 shows that normalized channel steepness for river reaches upstream of the top knickpoint, between knickpoints and between the fault and the lower knickpoint. We expect k_{sn} to be linearly to sublinearly correlated with rock uplift rates, assuming that the river in the lower reach near the fault is keeping pace with the local tectonic boundary conditions [*Kirby et al.*, 2003; *Wobus et al.*, 2006a; *Harkins et al.*, 2007; *Cyr et al.*, 2010; *DiBiase et al.*, 2010; *Miller et al.*, 2012]. Fault scarps are not observed where the study channels cut the fault [cf., *Cowie et al.*, 2008], so this latter assumption is reasonable. We therefore interpret the differences in k_{sn} upstream and along strike to reflect the erosional response of rivers in the

study area to an increase in fault throw rates as the fault segments grew and interacted. The high k_{sn} values in the lower reaches of the rivers just upstream of the fault reflect rivers steepening to keep pace with the new, larger fault throw rates following the linkage event that generated the lower set of knickpoints. The upper set of knickpoints tracks the footwall relief, so the "middle" reaches of the channels likely reflect river incision that matched the "old" prelinkage fault slip rates but where rates of down cutting have not yet adjusted to the current fault throw rates. Steepness indices in the headwaters are very low, which therefore reflect the relict landscape before substantial slip was accumulated on any of the basin-bounding faults.

Although the absolute magnitudes of k_{sn} are difficult to translate directly into fault throw rates [*Wobus et al*., 2006a; *Miller et al*., 2012; *Kirby and Whipple*, 2012], the relative magnitudes are instructive. If k_{sn} is linearly (or sublinearly) proportional to uplift rate, then the ratio between the k_{sn} upstream and downstream of the lower knickpoint (Figure 8) should reflect the ratio of throw rates before and after the change in fault uplift rate that generated the knickpoint. For the center of the Sperchios Fault system, the ratio of maximum k_{sn} values (Figure 8a, highlighted arrows) between the lower and middle reaches (~550 $m^{0.9}$ and 190 $m^{0.9}$, respectively) implies an increase in throw rates of approximately 3 times, assuming that k_{sn}~U. For the Coastal Fault (Figure 8b, arrows), the k_{sn} at the center of the fault between the lower and middle reaches (20 km along strike; Figure 8b) is ~340 $m^{0.9}$ and 60 $m^{0.9}$, respectively. The ratio of these values implies an increase in throw rates of up to 5 times, assuming k_{sn}~U. Similarly, if we compare the ratio of maximum lower reach k_{sn} for the center of the two fault systems, that in Sperchios Basin is greater than the Coastal Fault system by a factor of 1.6 times; this would reflect the relative throw rate difference between the two structures, all else being equal.

If fault interaction and linkage explains the generation of the lower knickpoint sets, then maximum fault slip rates have increased over time. This is important because while the measures of footwall relief and fault throw can be satisfactorily reconciled, existing throw rate and uplift rate constraints relative to sea level do not vary consistently along strike as one might expect. We suspect that these constraints differ because they employ fundamentally different methodologies (terrace data, coastal notches, and seismic constraints) and because they differ significantly in the time averaging used. A related question is when the fault interaction event occurred. To answer these two questions, we integrate our constraints on the footwall relief of the faults and the height of the knickpoints upstream of the active faults.

A minimum estimate of the footwall-uplift component of the total throw rate is to divide the footwall relief since the middle Pliocene (3.6 Ma), when we know the faults formed, by the time elapsed since. If the total throw is not known independently, a similar calculation for the throw rate requires us to know the relationship between the footwall relief and the throw. In general, the proportion of this total which is expressed in the footwall depends on a range of factors, including erosion of the footwall and sedimentation in the hanging wall [*Mirabella et al*., 2004; *Whittaker et al*., 2007b]. Here the data presented in Figure 4 suggest that for these fault systems, total throw is approximately 2–3 times the footwall relief. For the center of the Sperchios Fault (30 km along strike), the time-averaged throw rate since the Pliocene is 0.8–1.2 mm/yr, of which the footwall component relative to sea level is 0.4–0.5 mm/yr, and for the Coastal Fault, a similar calculation gives a throw rate of up to 0.4–0.6 mm/yr, of which the maximum footwall uplift component is 0.2–0.3 mm/yr.

However, these time-averaged estimates neglect any increase in fault throw rate, which is required to generate the lower set of knickpoints. The relative throw rate enhancement factor, E, along a linking fault array can be calculated from the length of the preexisting fault segments, L_i, and the distance from the midpoint of the ith segment to the nearest tip of the newly linked fault, R_i (see *Cowie and Roberts* [2001] for a full discussion). For a simple triangular displacement profile, this is calculated as

$$E = 2\,(R_i/L_i) \tag{3}$$

For the Sperchios Fault, the fault segments are approximately 20 km long (Figure 4). The central Kompotades fault segment therefore experienced an increase in throw rate of a factor of 3, assuming one linkage event to create a basin-bounding structure 60 km long. For the Coastal Fault zone, there are four fault segments which for simplicity we approximate as being 10 km long. Using the same approach, the central segments on the fault also increased their slip rate by approximately a factor of 3. We stress that these throw rate enhancement values, which are derived from fault interaction theory rather than geomorphology, are close to the ratios of normalized steepness indices (Figure 8) upstream

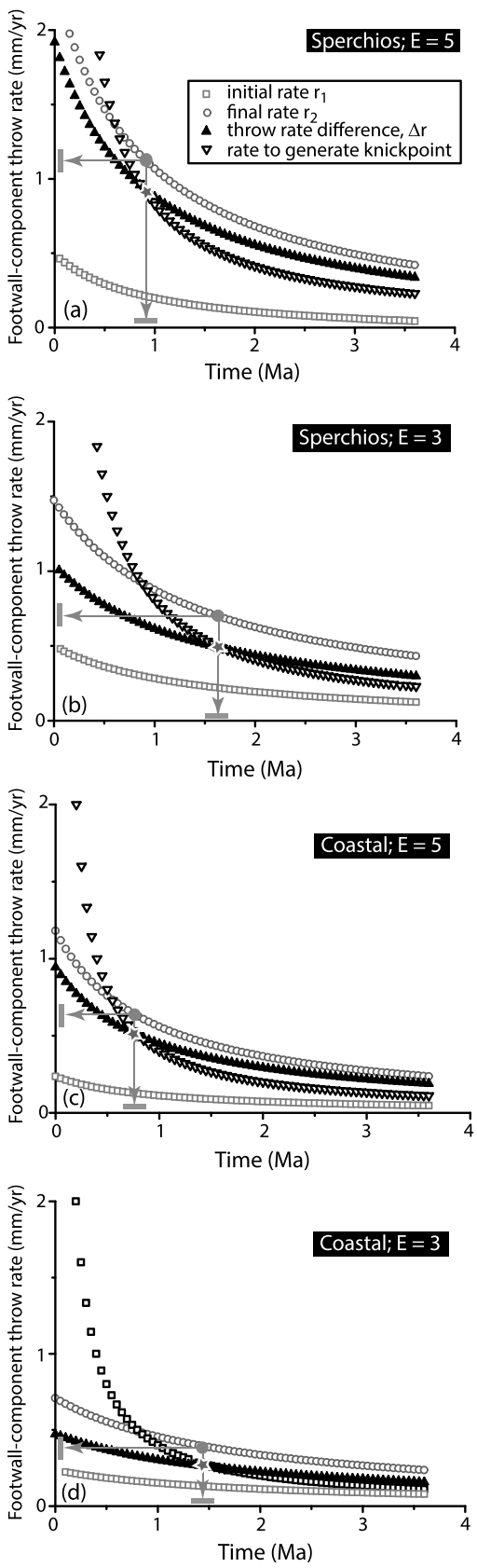

and downstream of the lower set of knickpoints, which we had independently used to estimate the increase in relative uplift rate felt by the rivers as a factor of 3–5 above.

As we argue that this throw rate increase can be explained by a single-linkage event for each fault system, we can therefore express the throw, D_v, since 3.6 Ma at the center of each of the fault systems as

$$D_v = r_1 t_1 + r_2 t_2 \tag{4}$$

where r_1 and r_2 are the throw rates before and after the linkage event, t_1 is the time between fault initiation and fault linkage, and t_2 is the time after the throw rate increase. Therefore, $t_1 + t_2 = 3.6$ Myr and $r_2 = Er_1$, where E is likely a factor of 3 but may be up to a factor of 5 for the Coastal Fault system using the channel steepness ratios extracted from Figure 8. Given an estimate of D_v, we can constrain the loci of times that a single slip rate increase could have occurred and the respective throw rates before and after linkage that would be implied (Figure 10, white squares and circles, respectively). Because the footwall relief component of the throw is better constrained than the absolute throw, which here is at least twice the footwall relief, we chose to use the former in the subsequent calculation.

This problem is solved graphically for the Sperchios (Figures 10a and 10b) and the Coastal (Figures 10c

Figure 10. Diagrams showing the calculation of current footwall component fault throw rate and fault linkage time for the center of the two fault systems, respectively, assuming that faults had initiated by 3.6 Ma. The white squares and circles show the locus of all possible footwall throw rates, prethrow (r_1) and postthrow (r_2) rate increases, assuming that a single fault linkage event generated the lower set of knickpoints on the study rivers and using a throw of 1750 and 850 m for the center of the Sperchios and Coastal Fault systems, respectively. The black triangles show the throw rate difference between these footwall component estimates, $\Delta r = r_2 - r_1$, for a linkage event happening at any time from 3.6 Ma to present. The inverted white triangles show the fault throw rate difference needed to generate the measured height of knickpoints at the center of the fault from 3.6 Ma to present. The best estimate for the actual footwall component throw rate and fault linkage time is where this rate coincides with the calculated throw rate difference prelinkage and postlinkage events (stars). (a) The Sperchios Fault system assuming a throw rate enhancement factor of 5. (b) The same as Figure 10a but assuming a throw rate enhancement factor of 3. (c) The Coastal Fault system assuming a throw rate enhancement factor of 5. (d) The same as Figure 10c but assuming a throw rate enhancement factor during of 3. The grey bars and arrows show the best fit footwall component throw rate and fault linkage time estimates derived from these calculations.

and 10d) Faults, where footwall relief in the center of the fault, D_v, is ~1750 m and ~900 m, respectively. For completeness, calculations with $E = 3$ and $E = 5$ are shown. For instance, Figure 9a shows that if a throw rate increase had occurred at 2 Ma on the Sperchios system and $E = 5$, the initial footwall component rate (white squares) would have been 0.15 mm/yr up to this point in time; afterward, it would have been 0.75 mm/yr. However, the footwall component of the fault throw rate post linkage, r_2, must also be consistent with the time needed to generate a knickpoint of a known vertical height, H, upstream of the fault since this linkage event [*Whittaker et al.*, 2008] (Figures 1b, 1c, and 1d) giving

$$H \sim t_2(r_2 - r_1). \tag{5}$$

This additional piece of information is enough to solve for t and r simultaneously, so using the lower knickpoint heights in the center of the two faults from Figure 6, we can estimate both the timing of fault linkage and the current footwall throw rate component in each case (Figure 10). For the Sperchios Basin, if the interaction event happened less than 1 Ma, the required rate of vertical knickpoint growth (inverted triangles) that would be needed to explain the current height of the knickpoints in the center of the fault is far higher than the throw rate difference implied by the fault interaction calculations above, for any throw rate enhancement factor in the range of 3–5 (Figures 9a and 9b). The opposite is true for fault linkage occurring before 2 Ma. Our results show that the best fit for $E = 5$ gives fault linkage and throw rate increase at ~0.9 ± 0.1 Ma, implying a current footwall uplift rate component at the center of the fault of 1.25 ± 0.1 mm/yr. A more realistic estimate, using a lower throw rate enhancement factor, $E = 3$, yields a linkage event at ~1.6 Ma and a footwall uplift rate of 0.75 ± 0.1 mm/yr. This is our preferred estimate because our fault interaction calculation and our k_{sn} ratios suggest that a factor of 3 is most appropriate.

For the Coastal Fault, if $E = 5$, we estimate that the fault linkage event occurred at ~0.7 Ma and that the footwall uplift rate is 0.6 ± 0.1 mm/yr. If $E = 3$, the fault segments became linked earlier at ~1.4 Ma, and the footwall uplift rate is 0.4 ± 0.1 mm/yr. Total throw rates in cases are 2–3 times the values above and therefore imply throw rates at the center of the Sperchios Fault zone of 1.5–2.2 mm/yr and 0.8–1.2 mm/yr at the center of the Coastal Fault zone, respectively, for $E = 3$. These calculations are consistent with the idea that the segment linkage event on the Coastal Fault system happened more recently than in the Sperchios Basin.

5.3. Assumptions, Applications, and Comparison With Existing Work

These calculations are approximations because we assume a single, instantaneous increase in throw rate on the fault as a result of fault interaction and linkage and because we assume the interaction of fault strands of initially equal length. Theoretical considerations, field and seismic evidence from the Italian Apennines and Turkey, suggest that changes in fault slip rate from linkage are generally rapid in geological terms [*Cowie and Roberts*, 2001; *Roberts and Michetti*, 2004; *Boulton and Whittaker*, 2009], so we feel that this assumption is a reasonable one. The throw rate enhancement factors derived ($3 \leq E < 5$) are consistent with changes in the ratio of cumulative displacement to fault segment length for multisegment interacting fault arrays [e.g., *Dawers and Anders*, 1995]. However, in fault systems with more complex segmentation patterns, a single L_i may not be appropriate. In theory, this method could be applied to any study location where fault throw is constrained or where footwall relief can be linked to variations in displacement along strike [e.g., *Mirabella et al.*, 2004]. Whereas previous studies on >100 km long Miocene to recent faults in the basin and range indicate that only footwall relief within 15 km of the fault tip is sensitive to fault throw rate [*Densmore et al.*, 2004], this study indicates that footwall relief can record fault throw for upper Pliocene to recent faults on the scale of 40–60 km, which are composed of segments <20 km long. Our approach would be most effective for faults on this scale, in which fluvial erodibility, climate, or fluvial erosion process did not differ significantly along strike. A final limitation is the time scale over which transient fluvial landscapes act as a "tape recorder" of the growth and interaction of faults [*Whittaker*, 2012]. This varies as a function of climate, lithology, and catchment size, and published estimates for this have varied by several orders of magnitude [*Whittaker et al.*, 2008; *Roberts and White*, 2010]. However, for catchments <100 km^2 on the scale of an individual normal fault block, field evidence for the Mediterranean region suggests that knickpoints can take 1–3 Ma to propagate through the landscape [*Whittaker et al.*, 2007a; *Whittaker and Boulton*, 2012].

The rates we obtain are consistent with, but extend, the coverage of existing geologic data. In the Sperchios Basin, existing estimates of time-averaged fault throw rates from stratigraphy are 1.1 mm/yr for the center of the basin [*Eliet and Gawthorpe*, 1995, 1996] (Figure 4, locality 1). We argue a somewhat higher rate of 1.5–2.2 mm/yr

on the central Kompotades since 1.6 Ma honors the geomorphic and geologic data most effectively. Our method can also be used to predict explicitly how throw rates will decline along strike of the faults toward the tips of the two systems, because accumulated throw and the throw rate enhancement factor both decline along strike away from the fault center. Assuming a triangular displacement profile, we suggest throw rates of 0.75–1 mm/yr for the center of the Sperchios and Thermopylae segments, respectively.

For the Coastal Fault, *Walker et al*. [2010] recently estimated a total fault throw rate of 1 mm/yr for the Kamena Vourla fault segment, which corresponds well with our throw rate estimate of 0.8–1.2 mm/yr throw rate, assuming $E = 3$ and a 1:1 or 2:1 partitioning of throw between the hanging wall and the footwall. A number of studies indicate that throw rates toward the edge of the western end of the Kamena Vourla segment and the eastern end of the Arkitsa segment are as little as 0.2 mm/yr [e.g., *Pirazzoli et al*., 1999; *Cowie et al*., 2008; *Goldsworthy and Jackson*, 2001; *Walker et al*., 2010] (Figure 4c, localities 1 and 5). We concur with these values, and our work therefore suggests that fault throw rates near the tip of Arkitsa segment must be less than the 1–2 mm/yr Holocene-only vertical uplift rates reported by *Cundy et al*. [2010] for the eastern end of the Arkitsa fault. Our estimates of fault linkage time here (0.8–1.4 Ma) is also in agreement with previous work [*Cowie et al*., 2008].

6. Conclusions

This paper uses a synthesis of quantitative geomorphology and fault interaction theory to estimate the throw rate and linkage times of active normal faults in the Northern Gulf of Evia and Sperchios Basin, Greece. We demonstrate that footwall relief varies systematically along strike of the two basin-bounding faults in the area and that it reflects fault segment lengths in each case. Although a simple relationship between footwall relief and fault throw does not always exist, for the faults studied here, variations in footwall relief generally reflect displacement and throw variations along strike, the latter of which is typically 2–3 times the footwall relief measured. Our data show that rivers crossing these faults are characterized by convex long profiles which often show two knickpoints, the vertical height of which varies systematically along strike and scales with the footwall relief on the active faults. The upper set of knickpoints have heights, measured from the fault, which are $>$85% of the maximum relief measured from topographic swath profiles, while the younger set of knickpoints, lying closer to the faults, have systematically lower elevations that also scale with the footwall relief.

The best explanation for these features is that the upper set of knickpoints record the growth of fault-bounded topography since the faulting started at approximately 3.6 Ma, while the lower knickpoints formed when the fault segments making up the Sperchios and Coastal Fault zones interacted and became linked, forming two longer structures of 60 km and 40 km length, respectively. These two linkage events led to an increase in the fault throw rate at the center of the two structures. The interpretation of a linkage event on each fault system is supported by the fact that for the lower set of knickpoints, the plan view distance that they have migrated upstream is predictably explained by catchment drainage area, indicating that each knickpoint set was generated together.

The throw rate enhancement factor at the center of the faults, due to linkage, is estimated to be a factor of 3–5 using two independent methods: the first compares the ratio of normalized steepness indices upstream and downstream of the lower knickpoints along the faults and the second uses a geometric approach based on the original length of the individual fault strands and the distance from the center of each segment to the tip of the newly linked structure [cf., *Cowie and Roberts*, 2001]. Moreover, because we know the footwall relief, we have some constraints on fault throw, and we have a minimum age for fault initiation (3.6 Ma); we can estimate what fault throw rates would be before and after any linkage event. The throw rate postlinkage must be consistent with the height and time needed to grow the documented knickpoints, so we use this additional condition to estimate the throw rate at the center of Sperchios and Coastal Fault systems. We estimate that the footwall uplift component of the throw rate in the Sperchios Fault is 0.75 mm/yr, implying an absolute throw rate of 1.5–2.2 mm/yr and a linkage time of ~1.6 Ma. For the Coastal Fault, a conservative estimate for the footwall uplift rate is 0.4 mm/yr, where the Kamena Vourla and Knimis fault segments meet, implying a maximum throw rate of 0.8–1.2 mm/yr following fault linkage at 0.8–1.4 Ma. These values bring greater clarity to recent estimates based on geodetic constraints and local terrace markers [e.g., *Walker et al*., 2010], allow fault slip rate variations to be constrained along strike, and placed in the context of fault growth history.

Acknowledgments
Whittaker and Walker were funded through the Department of Earth Science and Engineering, Imperial College London. We are very grateful for insightful reviews from Nancye Dawers, Editor Alex Densmore, and an anonymous reviewer. Data for the paper are presented in Tables 1 and 2. Further supporting information can be accessed from Alex Whittaker, a.whittaker@imperial.ac.uk.

References

Anders, A., M. Speigelman, and D. Rodgers (1993), The growth of fault bonded tilt blocks, *Tectonics*, *12*, 1451–1459, doi:10.1029/93TC01547.

Attal, M., G. Tucker, A. Whittaker, P. Cowie, and G. Roberts (2008), Modelling fluvial incision and transient landscape evolution: Influence of dynamic channel adjustment, *J. Geophys. Res.*, *113*, 1–16, doi:10.1029/2007JF000893.

Billiris, H., et al. (1991), Geodetic determination of tectonic deformation in central Greece from 1900 to 1988, *Nature*, *350*, 124–129.

Billiris, H., D. Paradissis, G. Veis, R. Davies, P. England, and B. Parson (1997), Geodetic strain of Greece in the interval 1892–1992, *J. Geophys. Res.*, *102*, 24, 571–24,588, doi:10.1029/97JB01644.

Boulton, S. J., and A. C. Whittaker (2009), Quantifying the slip rates, spatial distribution and evolution of active normal faults from geomorphic analysis: Field examples from an oblique-extensional graben, southern Turkey, *Geomorphology*, *104*, 299–316, doi:10.1016/j.geomorph.2008.09.007.

Clarke, P., et al. (1998), Crustal strain in central Greece from repeated GPS measurements in the interval 1989–1997, *Geophys. J. Int.*, *135*, 195–214.

Commins, D., S. Gupta, and J. Cartwright (2005), Deformed streams reveal growth and linkage of a normal fault array in the Canyonlands Graben, Utah, *Geology*, *33*, 645–648, doi:10.1130/G21433AR.1.

Cowie, P. A. (1998a), A healing-reloading feedback control on the growth rate of seismogenic faults, *J. Struct. Geol.*, *20*, 1075–1087.

Cowie, P. A. (1998b), Normal fault growth in three dimensions in continental and oceanic crust, in *Faulting and Magmatism at Mid-ocean Ridges*, *Geophys. Monogr. Ser.*, vol. 106, edited by R. Buck et al., pp. 325–348, AGU, Washington, D. C.

Cowie, P. A., and G. Roberts (2001), Constraining slip rates and spacings for active normal faults, *J. Struct. Geol.*, *23*, 1901–1915.

Cowie, P. A., M. Attal, G. E. Tucker, A. C. Whittaker, M. Naylor, A. Ganas, and G. Roberts (2006), Investigating the surface process response to fault interaction and linkage using a numerical modelling approach, *Basin Res.*, *18*, 231–266, doi:10.1111/j.1365-2117.2006.00298.x.

Cowie, P. A., A. C. Whittaker, M. Attal, G. Roberts, G. E. Tucker, and A. Ganas (2008), New constraints on sediment-flux dependent river incision: Implications for extracting tectonic signals from river profiles, *Geology*, *36*, 535–538, doi:10.1130/G24681A.1.

Crosby, B., and K. X. Whipple (2006), Knickpoint initiation and distribution within fluvial networks: 236 waterfalls in the Waipaoa River, North Island, New Zealand, *Geomorphology*, *82*, 16–38, doi:10.1016/j.geomorph.2005.08.023.

Cundy, A., K. Gaki-Papanastassiou, H. Maroukian, M. Frogley, and T. Cane (2010), Geological and geomorphological evidence of recent coastal uplift along a major Hellenic normal fault system (the Kamena Vourla fault zone, NW Evoikos Gulf, Greece), *Mar. Geol.*, *271*, 156–164, doi:10.1016/j.margeo.2010.02.009.

Cyr, A., D. Granger, V. Olivetti, and P. Molin (2010), Quantifying rock uplift rates using channel steepness and cosmogenic nuclide-determined erosion rates: Examples from northern and southern Italy, *Lithosphere*, *2*, 188–198, doi:10.1130/L96.1.

D'Arcy, M., and A. C. Whittaker (2014), Geomorphic constraints on landscape sensitivity to climate in tectonically active areas, *Geomorphology*, *204*, 366–381, doi:10.1016/j.geomorph.2013.08.019.

Davies, R., P. England, B. Parson, H. Billiris, D. Paradissis, and G. Veis (1997), Geodetic strain of Greece in the interval 1892–1992, *J. Geophys. Res.*, *102*, 24,571–24,588, doi:10.1029/97JB01644.

Dawers, N. H., and M. H. Anders (1995), Displacement-length scaling and fault linkage, *J. Struct. Geol.*, *17*, 607–614.

Densmore, A. L., N. H. Dawers, S. Gupta, P. A. Allen, and R. Gilpin (2003), Landscape evolution at extensional relay zones, *J. Geophys. Res.*, *108*(B5), 2273, doi:10.1029/2001JB001741.

Densmore, A. L., N. H. Dawers, S. Gupta, R. Guidon, and T. Goldin (2004), Footwall topographic development during continental extension, *J. Geophys. Res.*, *109*, F03001, doi:10.1029/2003JF000115.

Densmore, A. L., S. Gupta, P. A. Allen, and N. H. Dawers (2007), Transient landscapes at fault tips, *J. Geophys. Res.*, *112*, F03S08, doi:10.1029/2006JF000560.

DiBiase, R. A., and K. Whipple (2011), The influence of erosion thresholds and runoff variability on the relationships among topography, climate and erosion rate, *J. Geophys. Res.*, *115*, F04036, doi:10.1029/2011JF002095.

DiBiase, R. A., K. X. Whipple, A. M. Heimsath, and W. B. Ouimet (2010), Landscape form and millennial erosion rates in the San Gabriel Mountains, CA, *Earth Planet. Sci. Lett.*, *289*, 134–144, doi:10.1016/j.epsl.2009.10.036.

Eliet, P., and R. Gawthorpe (1995), Drainage development and sediment supply within rifts, examples from the Sperchios Basin, central Greece, *J. Geol. Soc.*, *152*, 883–893.

Eliet, P., and R. Gawthorpe (1996), Late Quaternary high resolution sequence stratigraphy of an active rift, the Sperchios Basin, Greece: An analogue for subtle stratigraphic plays, AAPG Bull., 5, CONF-960527- 1996, San Diego, Calif.

Finnegan, N., G. Roe, D. Montgomery, and B. Hallet (2005), Controls on the channel width of rivers: Implications for modelling fluvial incision of bedrock, *Geology*, *33*, 229–232, doi:10.1130/G21171.1.

Forzoni, A., J. E. A. Storms, A. C. Whittaker, and G. de Jager (2014), Delayed delivery from the sediment factory: A model to simulate the impact of catchment response time on sediment flux and fluvio-deltaic stratigraphy, *Earth Surf. Processes Landforms*, *39*, 689–704, doi:10.1002/esp.3538.

Goldsworthy, M., and J. Jackson (2000), Active normal fault evolution in Greece revealed by geomorphology and drainage patterns, *J. Geol. Soc.*, *157*, 967–981.

Goldsworthy, M., and J. Jackson (2001), Migration of activity within normal fault systems: Examples from the Quaternary of mainland Greece, *J. Struct. Geol.*, *23*, 489–506.

Goldsworthy, M., J. Jackson, and J. Haines (2002), The continuity of active fault systems in Greece, *Geophys. J. Int.*, *148*, 596–618.

Harkins, N., E. Kirby, A. Heimsath, R. Robinson, and U. Resier (2007), Transient fluvial incision in the headwaters of the Yellow River, northeastern Tibet, China, *J. Geophys. Res.*, *112*, F03S04, doi:10.1029/2006JF000570.

Hollenstein, C., M. Muller, A. Geiger, and H. Kahle (2008), Crustal motion and deformation in Greece from a decade of GPS measurements, 1993–2003, *Tectonophysics*, *449*, 17–40, doi:10.1016/j.tecto.2007.12.006.

Hopkins, M. C., and N. H. Dawers (2014), Changes in bedrock channel morphology driven by displacement rate increase during normal fault interaction and linkage, *Basin Res.*, doi:10.1111/bre.12072.

Howard, A. D., and G. Kerby (1983), Channel changes in badlands, *Geol. Soc. Am. Bull.*, *94*, 739–752.

Jackson, J. (1994), Active tectonics of the Aegean region, *Annu. Rev. Earth Planet. Sci.*, *22*, 239–271.

Jackson, J. (1999), Fault death: A perspective from actively deforming regions, *J. Struct. Geol.*, *21*, 1003–1010.

Jones, R., S. Kokkalas, and K. McCaffrey (2010), Quantitative analysis and visualization of non-planar fault surfaces using terrestrial laser scanning (LIDAR) – The Arkitsa fault, central Greece, as a case study, *Geosphere*, *5*, 465–482, doi:10.1130/GES00216.1.

Kirby, E., and K. Whipple (2001), Quantifying differential rock-uplift rates via stream profile analysis, *Geol. Soc. Am. Bull.*, *29*, 415–418.

Kirby, E., and K. Whipple (2012), Expression of active tectonics in erosional landscapes, *J. Struct. Geol.*, *44*, 54–75, doi:10.1016/j.jsg.2012.07.009.

Kirby, E., K. Whipple, W. Tang, and Z. Chen (2003), Distribution of active rock uplift along the eastern margin of the Tibetan Plateau: Inferences from bedrock river profiles, *J. Geophys. Res.*, *108*(B4), 2217, doi:10.1029/2001JB000861.

Kranis, H. D. (2007), Neotectonic Basin evolution in central-eastern mainland Greece: An overview, *Bull. Geol. Soc. Greece*, *40*, 60–373.

Le Pichon, X., and J. Angelier (1979), The Hellenic arc and trench system: A key to the evolution of the eastern Mediterranean area, *Tectonophysics*, *60*, 1–42.

Miller, S. R., S. L. Baldwin, and P. G. Fitzgerald (2012), Transient fluvial incision and active surface uplift in the Woodlark Rift of eastern Papua New Guinea, *Lithosphere*, *4*, 131–149, doi:10.1130/L135.1.

Mirabella, F., M. Ciaccio, M. Barchi, and S. Merlini (2004), The Gubbio normal fault (Central Italy): Geometry, displacement distribution and tectonic evolution, *J. Struct. Geol.*, *26*, 2233–2249.

Ouimet, W. B., K. X. Whipple, and D. E. Granger (2009), Beyond threshold hillslopes: Channel adjustment to base-level fall in tectonically active mountain ranges, *Geology*, *37*, 579–582, doi:10.1130/G30013A.1.

Pantosti, D., P. Martini, D. Papanastassiou, F. Lemeille, N. Palyvos, and G. Stavrakakis (2004), Paleoseismological trenching across the Atalanti fault (central Greece): Evidence for the ancestors of the 1894 earthquake during the middle ages and roman times, *Bull. Seismol. Soc. Am.*, *94*, 531–549.

Papanikolaou, I. D., G. Roberts, G. Deligiannakis, A. Sakellariou, and E. Vassilakis (2013), The Sparta Fault, Southern Greece: From segmentation and tectonic geomorphology to seismic hazard mapping and time dependent probabilities, *Tectonophysics*, *597–598*, 85–105, doi:10.1016/j.tecto.2012.08.031.

Petit, C., Y. Gunnell, N. Gonga-Saholiariliva, B. Meyer, and J. Seguinot (2009), Faceted spurs at normal fault scarps: Insights from numerical modelling, *J. Geophys. Res.*, *114*, B05403, doi:10.1029/2008JB00595.

Pirazzoli, P. A., S. C. Stiros, M. Arnold, J. Laborel, and F. Laborel-Deguen (1999), Late Holocenecoseismic vertical displacements and tsunami deposits near Kynos, Gulf of Euboea, central Greece, *Phys. Chem. Earth (A)*, *24*, 361–367.

Roberts, G. G., and N. White (2010), Estimating uplift rate histories from river profiles using African examples, *J. Geophys. Res.*, *115*, B02406, doi:10.1029/2009JB006692.

Roberts, G. P., and A. Ganas (2000), Fault-slip directions in central and southern Greece measured from striated and corrugated fault planes: Comparison with focal mechanism and geodetic data, *J. Geophys. Res.*, *105*, 23,443–23,462, doi:10.1029/1999JB900440.

Roberts, G. P., and A. M. Michetti (2004), Spatial and temporal variations in growth rates along active normal fault systems: An example from Lazio-Abruzzo, central Italy, *J. Struct. Geol.*, *26*, 339–376.

Roberts, G. P., P. Cowie, I. Papanikolaou, and A. M. Michetti (2004), Fault scaling relationships, deformation rates and seismic hazards: An example from Lazio-Abruzzo, central Italy, *J. Struct. Geol.*, *26*, 377–398.

Roberts, S., and J. Jackson (1991), Active normal faulting in central Greece: An overview, *Geol. Soc. London Spec. Publ.*, *56*, 125–142.

Sakellariou, D., G. Rousakis, H. Kaberi, V. Kapsimalis, P. Georgiou, T. Kanellopoulos, and V. Lykousis (2007), Tectono-sedimentary structure and late quaternary evolution of the North Evia Gulf Basin, Central Greece: Preliminary results, Proceedings of the 11th International Congress Athens, *Bull. Geol. Soc. Greece*, *37*(1), 451–462.

Tucker, G., and K. Whipple (2002), Topographic outcomes predicted by stream erosion models: Sensitivity analysis and inter-model comparison, *J. Geophys. Res.*, *107*(B9), 2179, doi:10.1029/2001JB000162.

Tucker, G. E., S. W. McCoy, A. C. Whittaker, G. P. Roberts, S. T. Lancaster, and R. Phillips (2011), Geomorphic significance of post glacial bedrock scarps on normal fault footwalls, *J. Geophys. Res.*, *116*, F01022, doi:10.1029/2010JF001861.

Tzanis, T., H. Kranis, and S. Chailas (2010), An investigation of the active tectonics in central-eastern mainland Greece with imaging and decomposition of topographic and aeromagnetic data, *J. Geodyn.*, *49*, 55–67, doi:10.1016/j.jog.2009.09.042.

Vassilakis, E., L. Royden, and D. Papanikolaou (2011), Kinematic links between subduction along the Hellenic trench and extension in the Gulf of Corinth, Greece: A multidisciplinary analysis, *Earth Planet. Sci. Lett.*, *303*, 108–120, doi:10.1016/j.epsl.2010.12.054.

Walker, R. T., S. Classie, M. Telfer, E. Nissen, P. England, C. Bryant, and R. Bailey (2010), Preliminary estimate of Holocene slip rate on active normal faults bounding the southern coast of the Gulf of Evia, central Greece, *Geosphere*, *6*, 583–593, doi:10.1130/GES00542.1.

Whipple, K. X., and G. E. Tucker (2002), Implications of sediment-flux dependent river incision models for landscape evolution, *J. Geophys. Res.*, *107*(B2), 2039, doi:10.1029/2000JB000044.

Whittaker, A. C. (2012), How do landscape record tectonics and climate?, *Lithosphere*, *4*, 160–164, doi:10.1130/RF.L003.1.

Whittaker, A. C., and S. J. Boulton (2012), Tectonic and climatic controls on knickpoint retreat rates and landscape response times, *J. Geophys. Res.*, *117*, F02024, doi:10.1016/j.geomorph.2008.01.018.

Whittaker, A. C., P. A. Cowie, M. Attal, G. E. Tucker, and G. P. Roberts (2007a), Bedrock channel adjustment to tectonic forcing: Implications for predicting river incision rates, *Geology*, *35*, 103–106, doi:10.1130/G23106A.1.

Whittaker, A. C., P. A. Cowie, M. Attal, G. E. Tucker, and G. P. Roberts (2007b), Contrasting transient and steady-state rivers crossing active normal faults: New field observations from the Central Apennines, Italy, *Basin Res.*, *9*, 529–556, doi:10.1111/j.1365-2117.2007.00337.x.

Whittaker, A. C., M. Attal, P. A. Cowie, G. E. Tucker, and G. P. Roberts (2008), Decoding temporal and spatial patterns of fault uplift using transient river long profiles, *Geomorphology*, *100*, 506–526.

Whittaker, A. C., M. Attal, and P. A. Allen (2010), Characterising the origin, nature and fate of sediment exported from catchments perturbed by active tectonics, *Basin Res.*, *22*, 809–828, doi:10.1111/j.1365-2117.2009.00447.x.

Wobus, C. W., K. Hodges, and K. X. Whipple (2003), Has focused denudation sustained active thrusting at the Himalayan topographic front?, *Geology*, *31*, 861–864.

Wobus, C. W., K. X. Whipple, E. Kirby, N. Snyder, J. Johnson, K. Spyropolou, B. Crosby, and D. Sheehan (2006a), Tectonics from topography: Procedures, promise, pitfalls, in *Tectonics, Climate and Landscape Evolution*, edited by S. Willett et al., *Geol. Soc. Am. Spec. Pap.*, *398*, 55–74.

Wobus, C. W., B. T. Crosby, and K. X. Whipple (2006b), Hanging valleys in fluvial systems: Controls on occurrence and implications for landscape evolution, *J. Geophys. Res.*, *111*, F02017, doi:10.1029/2005JF000406.

Wobus, C. W., G. E. Tucker, and R. Anderson (2006c), Self-formed bedrock channels, *Geophys. Res. Lett.*, *33*, L18408, doi:10.1029/2006GL027182.

